



OPEN ACCESS

EDITED BY

Xavier F. Figueroa,
Pontificia Universidad Católica de Chile, Chile

REVIEWED BY

Mauricio P. Boric,
Pontificia Universidad Católica de
Chile, Chile

Naidi Sun,
Beijing Institute of Technology, China

*CORRESPONDENCE

Graham M. Fraser,
✉ graham.fraser@mun.ca

RECEIVED 12 February 2025

ACCEPTED 27 May 2025

PUBLISHED 09 July 2025

CITATION

Kiley ME, Sové RJ, Smith RH, Wells BN, Russell
McEvoy GM and Fraser GM (2025)
Development of thin-film micro-outlets for
spatially constraining local PO₂ perturbations
to capillaries *in vivo*.
Front. Physiol. 16:1575776.
doi: 10.3389/fphys.2025.1575776

COPYRIGHT

© 2025 Kiley, Sové, Smith, Wells, Russell
McEvoy and Fraser. This is an open-access
article distributed under the terms of the
[Creative Commons Attribution License \(CC
BY\)](#). The use, distribution or reproduction in
other forums is permitted, provided the
original author(s) and the copyright owner(s)
are credited and that the original publication
in this journal is cited, in accordance with
accepted academic practice. No use,
distribution or reproduction is permitted
which does not comply with these terms.

Development of thin-film micro-outlets for spatially constraining local PO₂ perturbations to capillaries *in vivo*

Meghan E. Kiley¹, Richard J. Sové², Reilly H. Smith¹,
Brenda N. Wells¹, Gaylene M. Russell McEvoy¹ and
Graham M. Fraser^{1*}

¹Division of BioMedical Sciences, Faculty of Medicine, Memorial University of Newfoundland, St. John's, NL, Canada, ²Department of Biomedical Engineering, School of Medicine, Johns Hopkins University, Baltimore, MD, United States

Objective: To develop and validate thin-film micro-outlet devices to study microvascular blood flow responses to localized changes in skeletal muscle oxygen concentration ([O₂]).

Methods: 30 male Sprague-Dawley rats (159–194 g) were anesthetized and instrumented to maintain cardiovascular state. The extensor digitorum longus (EDL) muscle was dissected, isolated, and reflected over a gas exchange chamber (GEC) mounted in the stage of an inverted microscope. The GEC and EDL were coupled via a composite, gas permeable membrane, and a gas impermeable film fabricated with laser machined micro-outlets of specific diameters (200, 400, 600, and 1,000 μm). [O₂] in the EDL was dynamically manipulated with step-wise oscillations between 7% (1 min) → 12% (1 min) → 2% (1 min) → 7% (1 min), and step challenges from 7% (1 min) → 2% or 12% (2 min), while recording intravital video for capillary RBC oxygen saturation (SO₂) and hemodynamic measurements. Oxygen diffusion between tissue and micro-outlet devices was modelled using a finite element mass transport model to further validate experimental results.

Results: [O₂] oscillations imposed on capillaries directly overlying 400 μm micro-outlets caused significant changes in RBC SO₂ at 12% and 2% [O₂], compared to 7% [O₂] ($p < 0.0001$). [O₂] oscillations caused significant changes in capillary RBC supply rate (SR) at 2% [O₂] versus 7%, and were significantly different at 2% compared to 12% [O₂] ($p < 0.0014$). Similarly, [O₂] challenges imposed on capillaries overlying 200 μm micro-outlets also caused significant changes in RBC SO₂ at 2% [O₂], compared to 7% [O₂] ($p < 0.0001$), and caused significant changes in SR at 2% [O₂] compared to 7% ($p < 0.0001$).

Conclusion: Our composite thin-film devices were fabricated and validated to spatially confine oxygen perturbations to capillaries using micro-outlets of varying diameters. These results demonstrate that our devices

can manipulate capillary SO_2 and alter capillary RBC SR in vessels directly overlying the micro-outlet without affecting capillary SO_2 at a distance from the outlets. Our novel composite thin-film micro-outlet devices demonstrate that capillary blood flow responses can be provoked by manipulating $[\text{O}_2]$ in tissue regions as small as $\sim 200\ \mu\text{m}$ in diameter.

KEYWORDS

microcirculation, oxygen transport, blood flow regulation, capillary hemodynamics, microfluidic device

1 Introduction

Oxygen (O_2) mediated blood flow regulation is essential for meeting the metabolic demands associated with body organs and tissues (Duling and Berne, 1970a; Duling and Klitzman, 1980; Segal, 2005; Golub and Pittman, 2013). Under normal physiological conditions, energy is produced by oxidative phosphorylation in skeletal muscle to synthesize ATP, a process that requires a constant oxygen supply. To match ever-changing local oxygen demands in tissues, the arteriolar wall will vasodilate in response to low tissue O_2 concentration ($[\text{O}_2]$) to increase blood flow into capillary beds or vasoconstrict in response to high tissue $[\text{O}_2]$ (Duling, 1972; Pittman and Duling, 1973; Duling, 1974; Duling, 1973; Hutchins et al., 1974; Sullivan and Johnson, 1981; Jackson, 1986; Jackson et al., 1987; Dietrich et al., 2000; Ellis et al., 2005; Ngo et al., 2010).

The regulation of oxygen-mediated blood flow is highly localized and primarily driven by conditions within tissue microenvironments (Sparks, 1980; Renkin, 1985; Golub and Pittman, 2013). Regulatory mechanisms responsible for sensing flow changes to wall shear stress or vascular resistance from wall tension do not directly sense O_2 concentration levels or precisely regulate O_2 supply (Ellis et al., 2012; Schubert and Mulvany, 1999; Pohl et al., 2000; Carlson and Secomb, 2005). Several local mechanisms are likely responsible for this active regulation, and several have been proposed (as reviewed in Jackson, 2016). However, existing evidence fails to account for the sensitivity of vascular responses across the physiological range of tissue $[\text{O}_2]$ and at different scales (Duling and Berne, 1970b; Jackson and Duling, 1983; Messina et al., 1994; Pries et al., 1986; Ellsworth et al., 1995; Ellsworth et al., 2009; Jackson, 2016). Studies have been conducted over a wide range of partial pressure of oxygen (PO_2) conditions (10–150 mmHg) where some may not have physiological relevance at the site they are observed (Coburn et al., 1979; Tateishi and Faber, 1995a; Tateishi and Faber, 1995b; Kerkhof et al., 1999; Jackson, 2016).

Oxygen reactivity studies have been completed on various vessels along the vascular tree using a range of experimental techniques. These varied approaches may impact the responses observed depending on the vessel of interest, as described below. Evidence exists for potential O_2 sensors, including the parenchymal tissue, components of the vascular wall, and the red blood cells (Duling and Berne, 1970a; Pittman and Duling, 1973; Jackson and Duling, 1983; Hester, 1993; Pries et al., 1986; Ellsworth et al., 1995; Ellsworth, 2004; Sprague et al., 2009; Jackson, 2016). Controversial evidence exists on their involvement in arteriolar O_2 regulation,

but in the absence of the parenchyma in arterioles, O_2 responses are blunted (Jackson and Duling, 1983; Harder et al., 1996). There are *ex vivo* results that support vascular smooth muscle cells as the O_2 sensor, but when the endothelium is removed from arterioles and feed arteries, O_2 reactivity becomes blunted or diminished entirely (Frisbee et al., 2002; Messina et al., 1992; Tateishi and Faber, 1995a; Tateishi and Faber, 1995b; Kerkhof et al., 1999). Additionally, *in vivo* studies on hamster cheek pouches provided evidence that none of the arteriolar wall components directly sense O_2 changes (Jackson et al., 1987; Duling, 1974). However, data collected by pressure myography supports endothelial cells' participation in the O_2 reactivity response (Busse et al., 1983; 1984; Pohl and Busse, 1989; Jackson et al., 1987; Messina et al., 1992; 1994; Fredricks et al., 1994; Ward, 1999; Frisbee, 2001; Frisbee and Stepp, 2001; Frisbee et al., 2001; Frisbee et al., 2002). Considering the differences in the vasculature used to obtain this experimental evidence is essential. *Ex vivo* studies, for example, have focused on first-order arterioles and arteries, whereas intravital studies utilize small, third-to-fifth-order arterioles. Given the range of contemporary methodologies, it is important to develop appropriate experimental techniques to study microvascular blood flow regulation to confirm oxygen-associated mechanisms without interacting with responses in higher-order vessels.

Strong evidence exists in the literature to support red blood cells (RBCs) as the O_2 sensor (Bergfeld and Forrester, 1992; Stein and Ellsworth, 1993; Ellsworth et al., 1995; Ellsworth, 2004; Ellsworth et al., 2009; Jia et al., 1996; Stamler et al., 1997; Patel et al., 1999; Jagger et al., 2001). RBCs have the cellular machinery to detect PO_2 changes and initiate regulatory mechanisms, as they are mobile carriers of O_2 , and have been shown to release ATP, a vasodilatory molecule capable of increasing blood flow in response to O_2 depletion (Delp, 1999; Olsson, 1981; Bergfeld and Forrester, 1992; Rowell, 2004; Ellsworth et al., 1995; Jagger et al., 2001; Laughlin et al., 2012). It has been proposed that RBCs regulatory actions are initiated by hemoglobin conformational changes that occur when there is a reduction in RBC SO_2 (Bergfeld and Forrester, 1992; Stein et al., 1993; Ellsworth et al., 1995; Jagger et al., 2001; Buehler and Alayash, 2004; Ellsworth et al., 2009). This allosteric alteration initiates a signal transduction pathway in RBCs, increasing ATP release and transportation through pannexin-1 channels to bind P_2Y_2 receptors on the vascular endothelium (Sprague et al., 1996; McCullough et al., 1997; Collins et al., 1998; Dietrich et al., 2000). Then, an upstream vasodilatory response occurs by triggering hyperpolarization conducted via gap junctions between endothelial cells, transducing an ATP signal from capillary beds across the arteriolar tree (Jackson et al., 1987; Segal, 1994; Sprague et al.,

1996; McCullough et al., 1997; Collins et al., 1998; Welsh and Segal, 1998; Dietrich et al., 2000).

Therefore, it has been further hypothesized that SO_2 -dependent ATP release from RBCs is initiated at the capillary level (Bergfeld and Forrester, 1992; Stein and Ellsworth, 1993; Ellsworth et al., 1995; McCullough et al., 1997; Stamler et al., 1997; Ellsworth, 2004; González-Alonso, 2012; Ellsworth et al., 2009; Ellis et al., 2012). Capillary beds are the most direct site for communicating tissue oxygen needs as the RBC membrane is in closest proximity to the endothelium compared to venules and arterioles (Ellis et al., 2012). This provides the shortest possible diffusion distance between capillary endothelium and RBCs resident in the capillary lumen allowing for ATP to rapidly diffuse and bind to endothelial purinergic receptors (Ellis et al., 2012). Capillary endothelial cells are indeed electrically coupled and can communicate electrical signals to the upstream arterioles (Bagher and Segal, 2011). In support of this hypothesis, several studies have shown that conducted signaling along capillaries can occur *in vivo* (Lamb et al., 2021; Collins et al., 1998; Dietrich, 1989; Dietrich and Tyml, 1992; Song and Tyml, 1993), and in the case of oxygen mediated responses, are dependent on connexin40 to conduct hyperpolarization to upstream arterioles (Kowalewska et al., 2024).

Intravital video microscopy (IVVM), which allows for monitoring and recording of real-time blood flow hemodynamics, has been frequently used to study blood flow in relation to O_2 transport and sensing in microvascular networks (Dietrich and Tyml, 1992; Duling and Berne, 1970a; Potter et al., 1993; Welsh and Segal, 1998; Frisbee and Lombard, 2002; Frisbee et al., 2002). Using IVVM, O_2 -mediated blood flow can be studied within an intact system with multiple levels of vasoactive control during various experimental manipulations, such as altering tissue $[\text{O}_2]$ or locally micro-pipetting vasoactive stimuli onto an individual microvessel (Duling and Berne, 1970b; 1974; Jackson and Duling, 1983; Song and Tyml, 1993; Potter et al., 1993; Welsh and Segal, 1998; Frisbee and Lombard, 2002; Riemann et al., 2011). To confirm whether O_2 sensing, and regulation occurs at the capillary level, related IVVM approaches were developed to gain additional insights into this vascular level (Ellis et al., 2012; Ghonaim et al., 2011; 2021; Sové et al., 2021; Russell McEvoy et al., 2021; Russell McEvoy et al., 2022). Specifically, a gas exchange chamber setup was used to alter the PO_2 of an entire tissue surface, or in a microscale region of the rat extensor digitorum longus (EDL) muscle to stimulate microvascular networks and to observe their regulatory responses (Ellis et al., 2012; Ghonaim et al., 2011; 2021; Sové et al., 2021; Russell McEvoy et al., 2022; Kowalewska et al., 2024).

Gas-based micro-outlet devices fabricated to visualize highly localized responses at the microvascular level have shown promising results for the proposed SO_2 -dependent ATP-release mechanism of O_2 regulation (Ellis et al., 2012; Ghonaim et al., 2011; 2013; 2021; Sové et al., 2021). Such devices aim to have the spatial specificity required to quantify individual capillary RBC hemodynamic responses to $[\text{O}_2]$ manipulations with limited interactions of nearby vasculature (Ghonaim et al., 2011; 2021; Sové et al., 2021). If the proposed mechanism is correct, this direct capillary perturbation helps assess if an ATP signal generated in individual capillary networks when O_2 levels are depleted can initiate a conducted regulatory response upstream (Ghonaim et al., 2011; 2013). Micro-outlets with 100- μm diameters have been shown to

effectively alter SO_2 in single capillaries but not to provoke a blood flow response (Ghonaim et al., 2011). Although, larger micro-outlets that stimulated multiple capillaries obtained flow responses simultaneously with RBC SO_2 changes (Ghonaim et al., 2021; Sové et al., 2021). However, mathematical models developed to aid in the interpretation for these devices did not consider the diffusive spread of O_2 within the device's exchange membrane, which was a novel insight in recent experimental work (Ghonaim et al., 2011; 2013; 2021; Sové et al., 2021). This limitation in the model underestimated the radial diffusion from our devices, meaning the area stimulated by $[\text{O}_2]$ perturbations was effectively larger than expected; resulting in poorer spatial specificity than was originally intended (Ghonaim et al., 2011; 2021; Sové et al., 2021). Therefore, determining the location for O_2 sensing using fine spatial specificity of targeted O_2 perturbations to micro-scale tissue regions remains incomplete (Ghonaim et al., 2011; 2013; 2021; Sové et al., 2016; Sové et al., 2021).

In this study, we aimed to develop and validate a thin-film micro-outlet device with improved spatial specificity to localize oxygen perturbations at the capillary level in skeletal muscle. An improvement from previous implementations, our device is designed to offer superior optical characteristics allowing for distortion-free visualization and analysis of capillaries being manipulated. This allows for capillaries directly overlying the micro-outlet, and at a distance from the outlet edge, to be recorded with IVVM simultaneously (Ghonaim et al., 2011; 2013; Sové et al., 2021). Our overarching hypothesis is that SO_2 -dependent ATP release from erythrocytes is a major mechanism of oxygen-mediated blood flow regulation that is initiated at the capillary level. We sought to test the spatial specificity of this response by fabricating circular micro-outlets of different diameters coupled to a microfluidic gas exchange chamber. We used micro-outlet devices to spatially target groups of capillaries in live muscle tissue with a range of $[\text{O}_2]$ perturbations with quantification of the resulting microhemodynamic responses. Furthermore, we validated our approach by applying an established mathematical model to predict PO_2 conditions within the tissue and the oxygen permeable layers of our device, demonstrating a high degree of spatial specificity of imposed O_2 perturbations. The current work redefines the critical scale for O_2 sensing in skeletal muscle microcirculation, and provides further evidence for the role of capillaries in initiating highly localized O_2 -mediated blood flow regulatory responses.

2 Methods

2.1 Design and fabrication of the 3D printed gas exchange chamber

The design of the gas exchange chamber (GEC) was adapted from previously reported computer-aided designs (Sové et al., 2021). Modifications of the GEC components used in this study were made using Tinkercad (Tinkercad.com, Accessed January 2021–September 2021). The GEC components consisted of a 110 mm diameter 3D printed stage insert base designed to fit the microscope stage cutout, with a micro gas channel formed between a 45 × 55 mm glass coverslip, a 0.15 mm thick 3D printed gas channel gasket, and an overlying 3D printed top plate (Figure 1). The top plate

contained integral inlet and outlet ports to connect the GEC channel to the gas supply. The composite micro-outlet device membrane, described below, was mounted above a 4.5×6.5 mm exchange window fabricated in the top plate to allow coupling of the micro-outlet device with the GEC gas channel (Figure 1). The assembled device was sealed with adhesive vinyl sheets and connected by plastic tubing to a triple-inlet manifold supplied by three computer-controlled mass flow meters (SmartTrak100, Sierra Instruments, Monterey, CA, United States) for each gas channel (CO_2 , N_2 , O_2), with a frequency response of <300 ms.

2.2 Micro-outlet device fabrication

2.2.1 Fabrication of micro-outlets

Polyvinylidene chloride film (PVDC) (Asahi Wrap, Asahi Kasei, Tokyo, Japan) was used as the gas-impermeable layer in a composite membrane micro-outlet device. Micro-outlet holes were laser cut into PVDC film using high-precision laser cutting (Universal Laser Systems—Model # ILS12-150D) at 100% speed and 0.1% power on a single laser using high-precision cuts. Four micro-outlet tessellations designed for each outlet diameter were laser cut into gas impermeable PVDC film, with $1,000 \mu\text{m}$ of solid film separating each outlet cut. Each micro-outlet tessellation was patterned to fit within the perimeter of the 4.5×6.5 mm exchange window of the 3D printed GEC top plate (Figure 1). The tessellation pattern varied according to the diameter of micro-outlets used, with $200 \mu\text{m}$ outlets machined in a 5×4 (rows \times columns) pattern, $400 \mu\text{m}$ and $600 \mu\text{m}$ outlets were machined in a 4×3 pattern, and $1,000 \mu\text{m}$ outlets were machined in a 3×2 pattern. To facilitate handling and subsequent spin coating of the PDMS membrane layer onto the PVDC film, each tessellation pattern was cut in the center of a 25×75 mm laser-cut piece of PVDC film. The micro-outlets cut into the PVDC film were inspected under a stereo microscope and thoroughly cleaned using 70% isopropyl solution and distilled water. A glass microscope slide was similarly cleaned and the 25×75 mm PVDC film containing the micro-outlet tessellation was carefully placed and smoothed onto a glass slide using 2–3 drops of distilled water and then left to dry in preparation for spin coating. The water droplets help to tightly adhere the PVDC film to the glass slide and prevent air bubbles from forming between the glass and film.

2.2.2 Fabrication of composite gas exchange membranes

Gas impermeable laser-cut micro-outlet PVDC membranes were bonded to gas-permeable polydimethylsiloxane (PDMS) to create a composite device for spatially constrained gas exchange. A 10:1 (15 g:1.5 g) mixture of PDMS base and curing agent (Dow Corning, Midland, MI) was weighed and vigorously mixed for 2 min as directed by the manufacturer's instructions. The PDMS mixture was degassed in a vacuum chamber three consecutive times for 10 min. Once degassed, the mixture was coated on top of a glass microscope slide with a micro-outlet film and spun coat for 30 s at $1,000$ rpm. Following spin coating, the slide was transferred into a vacuum chamber for 10 min of degassing to ensure no bubbles were present in the PDMS covering the micro-outlet holes. The microscope slides and composite membrane were placed on a hot plate at 80°C for 20 min to initiate the curing of PDMS. After

heating, the slide was covered with an inverted Petri dish to prevent dust particles from adhering to the device and left for 24 h to allow for complete curing of the PDMS. Once PDMS was cured on the PVDC film layer, the composite device was slowly peeled off the slide to ensure the delicate PDMS-filled micro-outlet holes remained intact. Once this was achieved, the composite device was placed directly over top of the 3D printed GEC top plate to align the tessellation pattern with the 3D printed window. The extra material of the composite membrane outside of the micro-outlet tessellation was trimmed, and the membrane was secured using double-sided tape and clear adhesive vinyl to ensure the composite micro-outlet device was fully sealed with the GEC.

2.3 Animal protocol

2.3.1 Instrumentation and physiological monitoring

30 male Sprague-Dawley rats (159–194 g) were obtained from Charles River Laboratories and housed in Animal Care Facilities allowing them to acclimatize over a 5–7-day period before testing. Rats were fed Teklad 2018 (Envigo, Indianapolis, IND, United States) standard rodent chow. All animal protocols were approved by Memorial University Animal Care Committee.

To begin, animals were anesthetized using sodium pentobarbital (Euthanyl, Bimeda, Cambridge, ON, Canada) at 65 mg/kg through intraperitoneal injection. Following induction and prior to surgery, depth of anesthesia was assessed through palpebral reflex and the absence of withdrawal or reaction following firm toe pinch on the left foot. The animal was transferred to the surgical field and a rectal temperature probe was inserted to monitor body temperature. The animal's core temperature was maintained between 36°C and 37°C throughout the experiment using a heating pad and/or a heat lamp as needed.

An incision was made between the clavicle and the jaw along the midline to allow for instrumentation as previously described (Tyml and Budreau, 1991; Fraser et al., 2012). Briefly, the left common carotid artery was blunt dissected and isolated for cannulation to allow for continuous monitoring and recording of blood pressure and heart rate (400a Blood Pressure Analyzer, Micro-Med, Louisville, KY, United States). The jugular vein was blunt dissected, isolated, and cannulated to deliver heparinized saline for fluid resuscitation (2 mL/kg/hr) via an infusion pump (PhD 2000, Harvard Apparatus, Holliston, MA, United States). The depth of anesthesia was assessed frequently by checking the animal's blink response, monitoring heart rate variability, and mean arterial blood pressure changes. Supplemental anesthetic (22 mg/kg) was administered via the jugular cannula as required. Animals were tracheotomized and mechanically ventilated (Inspira ASV, Harvard Apparatus, Holliston, MA, United States) with a FiO_2 of $\sim 30\%$ O_2 balanced with N_2 . Respiratory rate and volume were determined based on the animal's weight per the manufacturer's instructions. The right EDL, a muscle in the lower hindlimb of the rat, was blunt dissected and isolated from overlying connective tissue, as previously described (Fraser et al., 2012; Tyml and Budreau, 1991). The distal tendon of the EDL was cut, the muscle was lifted and carefully rinsed with warm saline before being reflected over the objective on the stage of an inverted microscope (Olympus

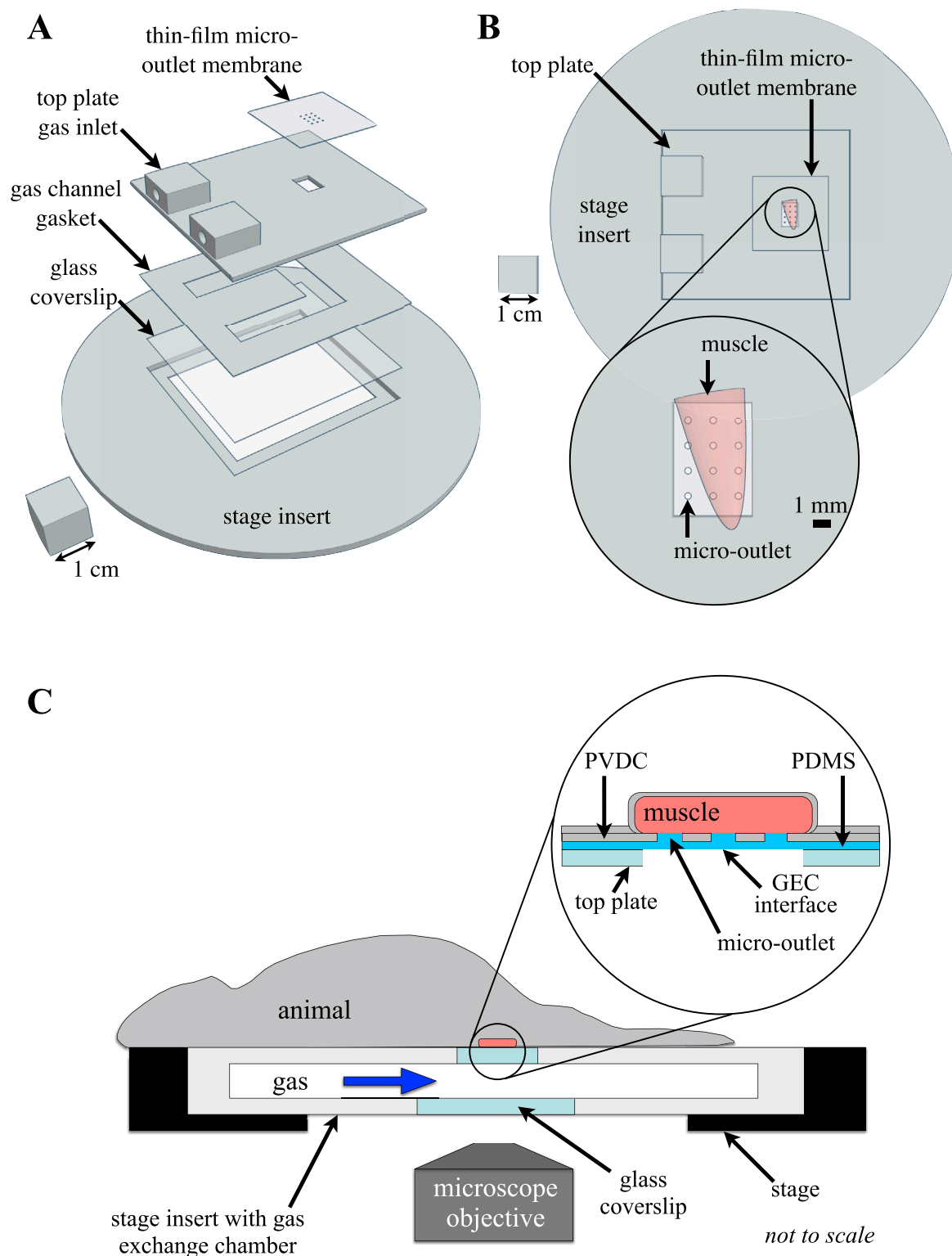


FIGURE 1

Experimental setup of the thin-film micro-outlet device and gas exchange chamber (GEC). The 3D printed GEC is fabricated to fit in the inverted microscope stage, with the extensor digitorum longus (EDL) muscle aligned directly over the thin-film micro-outlet device membrane. (A) shows an exploded view of the computer-aided design model of the GEC components illustrating device assembly. Top view of the assembled GEC with the EDL muscle overlying a 400 μm micro-outlet tessellation is shown in (B). Micro-outlets were laser machined in polyvinylidene chloride (PVDC) barrier film which was coupled with polydimethylsiloxane (PDMS) to allow for diffusion between the GEC interface and the tissue overlying each micro-outlet. The top surface and sides of the muscle are isolated from room air by covering with a rectangle of gas-impermeable polyvinylidene chloride film and finally covered with a glass coverslip (not shown), ensuring the muscle is only affected by gases flowing through the chamber ((C) adapted from Sové et al., 2021, used under Creative Commons License).

IX73, Tokyo, Japan). The EDL was carefully positioned over the exchange window of the 3D-printed stage insert. To improve optical coherence, the muscle was gently compressed using a cover slip with two beads of vacuum grease (Dow Corning, Midland, MI, United States), and a microscope slide similarly prepared with parallel beads of vacuum grease. The EDL was covered with PVDC film for isolation from the outside environment (Saran, Dow Corning, MI, United States) and bathed in warm saline. The muscle surface overlying the microscope objective was interfaced with the GEC gas channel via the PDMS-filled micro-outlet holes within the composite device membrane. The animal was allowed to equilibrate on the microscope stage for 30 min after EDL positioning and setup were complete. Following equilibration and when the animal's body temperature was between 36°C–37°C, and MAP was above 80 mmHg, an arterial blood sample was collected to measure blood gases (VetScan iSTAT, Abbott Point of Care Inc., Princeton, NJ, United States). The partial pressure of oxygen (PO_2) and carbon dioxide (PCO_2) was maintained at physiological levels, and the ventilation rate and volume were adjusted to maintain blood gases within the normative range.

2.4 Offline analysis using custom MATLAB software

Recorded digital video sequences were processed using a graphical user interface (GUI) driven custom program written in MATLAB (Mathworks, Natick, Mass, MA, United States). This processing software creates functional images for vessel selection and generates MP4 videos that help identify in-focus vessels for selection and analysis in the custom MATLAB software (Fraser et al., 2012; Ellis et al., 1990; 1992; 2012; Japee et al., 2004; Ghonaim et al., 2021). The analysis GUI measures capillary RBC hemodynamics and capillary RBC oxygen saturation (SO_2) as has been described previously (Fraser et al., 2012; Ellis et al., 1990; 1992; 2012; Japee et al., 2004). Output from the analysis software underwent further structured quality control to exclude spurious values that can result from poor vessel delineation or out-of-focus segments.

2.5 Hemodynamic and oxygen saturation measurements

Time-dependent capillary RBC hemodynamic (velocity, supply rate, and hematocrit) and SO_2 measurements were collected for capillaries during step-wise $[O_2]$ oscillations between 7% (1 min) \rightarrow 12% (1 min) \rightarrow 2% (1 min) \rightarrow 7% (1 min), high $[O_2]$ challenges from 7% (1 min) \rightarrow 12% (2 min), and low $[O_2]$ challenges from 7% (1 min) \rightarrow 2% (2 min). For measurements obtained during 4-min $[O_2]$ oscillations, the mean for each data channel was calculated for the first minute at 7% $[O_2]$, and for the last 15 s for each subsequent 1-min period at 12%, 2%, and 7% $[O_2]$. Similarly, for $[O_2]$ challenges, means were calculated for the first minute at 7% $[O_2]$, and for the last 15 s of the 2-min challenge period.

Capillary data for each micro-outlet size tested was sorted into four bins based on the location of analyzed capillary segments relative to the micro-outlet. The first bin included capillary segments

'inside' the micro-outlet, meaning the segments were directly overlying the micro-outlet surface and were resolved inside the perimeter of the laser machined hole in the PVDC layer. Data from capillary segments located 'outside' the micro-outlet was binned into three distance ranges: $<100\ \mu\text{m}$, $100\text{--}200\ \mu\text{m}$, and $>200\ \mu\text{m}$ from the perimeter of the laser-machined hole in the PVDC layer. To facilitate distance measurements, the outline and mid-point of each analyzed capillary segment was annotated on functional images generated from the video sequences. Distances of each capillary segment's mid-point to the perimeter of the micro-outlet hole were measured from the annotated functional images using ImageJ software (Rasband, W.S., ImageJ, U. S. National Institutes of Health, Bethesda, Maryland, United States, <https://imagej.nih.gov/ij/>, 1997–2018) and vessels were assigned to the appropriate distance bin. Hemodynamic measurements from capillaries crossing the micro-outlet with connected segments both 'inside' and 'outside', were only included in the 'inside' bin. Similarly, SO_2 measurements from capillaries crossing the micro-outlet were only included in 'outside' bins if the segment was flowing towards the micro-outlet.

Capillary hemodynamic and SO_2 measurements were sorted based on temporally paired measurements from $[O_2]$ oscillation and $[O_2]$ challenge data. Statistical comparisons were made for each imposed $[O_2]$. For $[O_2]$ oscillations, normally distributed capillary data were paired across the four $[O_2]$ of the oscillation, and repeated measures one-way analysis of variance (ANOVA) with Holm-Šidák's multiple comparisons test was used to identify significant differences between each $[O_2]$ condition. Non-normally distributed $[O_2]$ oscillation capillary data were grouped by $[O_2]$, and Friedman tests with Dunn's multiple comparison post-test were used to identify significant differences between each $[O_2]$ condition of the oscillation. For $[O_2]$ challenges, normally distributed capillary data were paired across the two $[O_2]$ conditions, and a paired t-test was used to identify significant differences between the baseline period and end of the challenge. Non-normally distributed $[O_2]$ challenge capillary data were grouped by $[O_2]$, and a Wilcoxon test was used to identify significant differences between the baseline and end of the challenge. A p value of <0.05 was considered significant across all comparisons. All tests were completed using Prism 9 (GraphPad Prism Software, LLC, 9.2.0 (283)). Means and standard deviations are reported in the results section unless otherwise noted.

2.6 Mathematical model of tissue oxygenation

A mathematical model of oxygen diffusion was used to determine the expected PO_2 within the tissue for the specific conditions imposed experimentally using the gas exchange chamber. Oxygen diffusion within the overlying muscle tissue and layers of the micro-outlet device were simulated using a finite element model similar to that described previously (Sové et al., 2021; Russell McEvoy et al., 2021). PO_2 in the system was determined by numerically solving:

$$\nabla \cdot (D_{PDMS} \cdot k_{PDMS} \cdot \nabla p) = 0,$$

in the PDMS layer,

$$\nabla \cdot (Dk_{PVDC} \cdot k_{PVDC} \cdot \nabla p) = 0,$$

in the PVDC layer, and

$$\nabla \cdot (D_{\text{tissue}} \cdot k_{\text{tissue}} \cdot \nabla p) + q \left(1 - \frac{p}{p_b} \right) - M_0 \frac{p}{p + p_{50}} = 0,$$

in the tissue, where M_0 is the maximal tissue oxygen consumption, p_{50} is the PO_2 at which consumption is half M_0 , p_b is the effective capillary PO_2 and q is the rate of oxygen transport from the capillaries into the tissue. D and k are the oxygen diffusivity and solubility in the medium denoted by the subscript. The model parameter values and associated references are listed in [Supplementary Table S1](#). Fixed value boundary conditions for PO_2 were prescribed at the interface of the system with the gas exchange chamber (see [Figure 1](#)), and zero flux boundary conditions were specified on all other boundaries of the volume. The governing equations were discretized using a finite volume approach and the resulting system of equations was solved iteratively by successive overrelaxation.

3 Results

3.1 Optical characteristics of thin-film micro-outlets

The thin-film micro-outlet devices fabricated for the current study produced superior optical clarity compared to previous devices using glass substrates. Our current approach of spin coating PDMS onto PVDC films containing laser machined micro-outlets allows for capillaries in the same focal plane, both overlying the micro-outlet and at a distance, to be clearly resolved simultaneously ([Figure 2](#)).

3.2 Systemic physiological measurements

Systemic physiological measurements were taken for each animal and means are reported for each group according to micro-outlet diameter size as shown in [Table 1](#). Similarly, blood gas samples were collected for each animal and are displayed in [Table 2](#) grouped based on corresponding micro-outlet diameter sizes.

3.3 400 μm micro-outlet oxygen oscillation data

$[\text{O}_2]$ oscillations imposed on capillaries directly overlying 400 μm micro-outlets caused significant changes in capillary RBC SO_2 at 12% GEC $[\text{O}_2]$, $85.9\% \pm 9.6\%$, and 2% GEC $[\text{O}_2]$, $43.2\% \pm 14.8\%$, compared to baseline 7% GEC $[\text{O}_2]$, $66.2\% \pm 13.2\%$ ($p < 0.0001$) ([Figure 3](#)). Imposed $[\text{O}_2]$ oscillations caused no significant changes in SO_2 in capillaries outside the micro-outlet edge ([Figure 4](#)).

$[\text{O}_2]$ oscillations imposed on capillaries directly overlying 400 μm micro-outlets caused significant changes in capillary hematocrit in capillaries overlying the outlet at 12% GEC $[\text{O}_2]$, $23.5\% \pm 10.1\%$ compared to 2% GEC $[\text{O}_2]$, $25.4\% \pm 9.7\%$ ($p = 0.005$) ([Figure 3](#)), but not in capillaries outside the outlet ([Figure 4](#)). $[\text{O}_2]$ oscillations imposed on capillaries directly overlying 400 μm

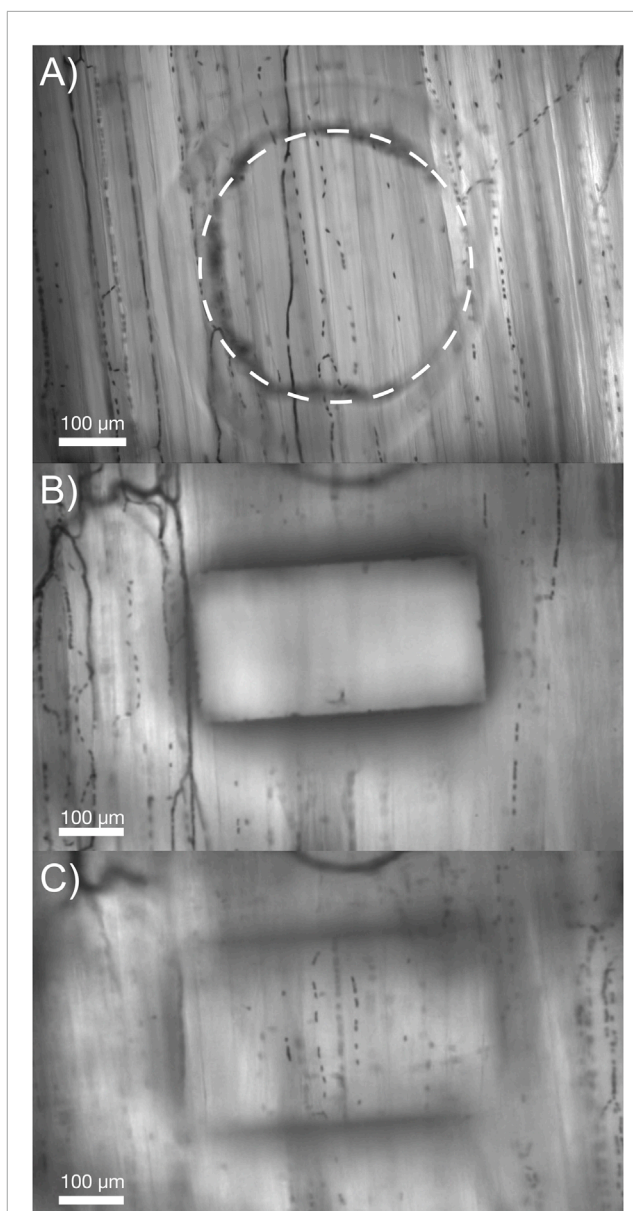


FIGURE 2
Comparison of the optical properties obtained in our micro-outlet device with a previous device used *in vivo*. (A) Image of our optically superior thin-film 400 μm micro-outlet device *in vivo*. (B,C) Images of a previous micro-outlet device demonstrating the inability to simultaneously visualize in-focus vessels overlying, and adjacent to the outlet. Images in (B,C) are courtesy of Dr. Chris Ellis' Lab at Western University, collected as part of the study by [Sové et al., 2021](#).

micro-outlets caused significant changes in capillary RBC velocity at 2% GEC $[\text{O}_2]$, $211.5 \pm 130.2 \mu\text{m/s}$, compared to baseline 7% GEC $[\text{O}_2]$, $187.4 \pm 134.2 \mu\text{m/s}$ and at 12% GEC $[\text{O}_2]$, $185.1 \pm 122.1 \mu\text{m/s}$ compared to 2% GEC $[\text{O}_2]$, $211.5 \pm 130.2 \mu\text{m/s}$ ($p < 0.0001$) ([Figure 3](#)). $[\text{O}_2]$ oscillations imposed on capillaries directly overlying 400 μm micro-outlets did not cause significant changes in capillary RBC velocity in vessels outside the micro-outlet ([Figure 4](#)).

$[\text{O}_2]$ oscillations imposed on capillaries directly overlying 400 μm micro-outlets caused significant changes in capillary RBC supply rate at 2% GEC $[\text{O}_2]$, $13.8 \pm 9.7 \text{ cells/s}$, and 7% GEC $[\text{O}_2]$,

TABLE 1 Mean and standard deviation of systemic animal data for each experimental group based on micro-outlet diameter size.

	200 μm outlets (N = 6)	400 μm outlets (N = 6)	600 μm outlets (N = 11)	1000 μm outlets (N = 7)
Animal Weight (g)	179.5 \pm 10.7	178.5 \pm 7.7	176.7 \pm 7.3	187.1 \pm 4.3
Mean arterial pressure (mmHg)	94.6 \pm 6.0	94.2 \pm 8.8	94.54 \pm 5.4	96.93 \pm 5.5
Systolic blood pressure (mmHg)	99.0 \pm 6.7	99.1 \pm 9.0	103.0 \pm 7.8	111.1 \pm 5.6
Diastolic blood pressure (mmHg)	87.9 \pm 5.4	87.2 \pm 8.9	84.0 \pm 6.8	82.0 \pm 5.4
Heart rate (beats/min)	411.9 \pm 21.2	403.0 \pm 24.8	394.6 \pm 20.7	399.2 \pm 16.8
Respiratory Rate (breaths/min)	83.5 \pm 1.4	83.3 \pm 1.2	83.8 \pm 0.9	82.4 \pm 0.5
Respiratory volume (cc)	1.20 \pm 0.07	1.18 \pm 0.05	1.17 \pm 0.06	1.24 \pm 0.03

TABLE 2 Mean and standard deviation of animal blood gas data for each experimental group based on micro-outlet diameter size used.

	200 μm outlets (N = 6)	400 μm outlets (N = 6)	600 μm outlets (N = 11)	1000 μm outlets (N = 7)
pH	7.40 \pm 0.03	7.42 \pm 0.02	7.43 \pm 0.05	7.42 \pm 0.04
PCO ₂ (mmHg)	50.0 \pm 3.8	45.8 \pm 3.5	46.4 \pm 6.6	48.3 \pm 5.8
PO ₂ (mmHg)	113.8 \pm 15.4	102.5 \pm 9.2	114.0 \pm 17.7	120.1 \pm 10.3
BEecf (mmol/L)	6.3 \pm 1.2	5.5 \pm 1.9	5.8 \pm 2.3	6.9 \pm 2.2
HCO ₃ (mmol/L)	29.4 \pm 4.4	29.8 \pm 1.8	30.1 \pm 2.1	31.3 \pm 2.4
SaO ₂ (%)	98.0 \pm 0.9	97.8 \pm 0.8	98.2 \pm 1.3	98.7 \pm 0.5
Lac (mmol/L)	0.87 \pm 0.40	0.87 \pm 0.21	1.01 \pm 0.68	1.01 \pm 0.43

Note: PCO₂: partial pressure of carbon dioxide; PO₂: partial pressure of oxygen; BEecf: base excess in the extracellular fluid compartment concentration; HCO₃: bicarbonate concentration; TCO₂: total carbon dioxide; SaO₂: arterial oxygen saturation; Lac: lactate concentration.

12.8 \pm 9.3 cells/s compared to baseline 7% GEC [O₂] 11.0 \pm 7.7 cells/s and at 12% GEC [O₂], 10.8 \pm 8.0 cells/s, compared to 2% GEC [O₂], 13.8 \pm 9.7 cells/s ($p < 0.0210$) (Figure 3). [O₂] oscillations using 400 μm micro-outlets did not cause significant changes in capillary RBC supply rate in vessels outside the micro-outlet (Figure 4).

3.4 400 μm micro-outlet oxygen challenge data

[O₂] challenges imposed on capillaries directly overlying 400 μm micro-outlets caused significant changes in capillary RBC SO₂ at 12% GEC [O₂], 84.7% \pm 8.5%, compared to baseline 7% GEC [O₂], 70.1% \pm 8.5% ($p < 0.0001$) (Figure 5). [O₂] challenges imposed on capillaries directly overlying 400 μm micro-outlets caused significant changes in RBC SO₂ at 2% GEC [O₂], 43.1% \pm 16.8%, compared to baseline 7% GEC [O₂], 69.1% \pm 12.1% ($p < 0.0001$) (Figure 7). Both high and low [O₂] challenges imposed on capillaries caused no significant change

in mean RBC SO₂ for capillaries outside the micro-outlet edge (Figures 6, 8).

[O₂] challenges imposed on capillaries directly overlying 400 μm micro-outlets caused a significant change in capillary hematocrit at 2% GEC [O₂], 25.7% \pm 9.4%, compared to baseline 7% GEC [O₂], 21.8% \pm 9.4% ($p < 0.0001$) but not at 12% GEC [O₂] (Figures 5, 7). High [O₂] challenges did not cause significant changes in capillary hematocrit for vessels at various distances from the outlet edge but there was a significant change at 2% GEC [O₂], 25.4% \pm 7.0%, compared to baseline 7% GEC [O₂], 22.8% \pm 7.6% for vessels greater than 200 μm away during low [O₂] challenges ($p = 0.0024$) (Figures 6, 8).

[O₂] challenges imposed on capillaries directly overlying 400 μm micro-outlets caused significant changes in capillary RBC velocity at 12% GEC [O₂], 157.0 \pm 84.4 $\mu\text{m/s}$, compared to baseline 7% GEC [O₂], 165.0 \pm 89.9 $\mu\text{m/s}$ ($p = 0.0426$) (Figure 5). [O₂] challenges imposed on capillaries directly overlying 400 μm micro-outlets caused significant changes in capillary RBC velocity at 2% GEC [O₂], 274.4 \pm 210.4 $\mu\text{m/s}$, compared to baseline 7% GEC [O₂],

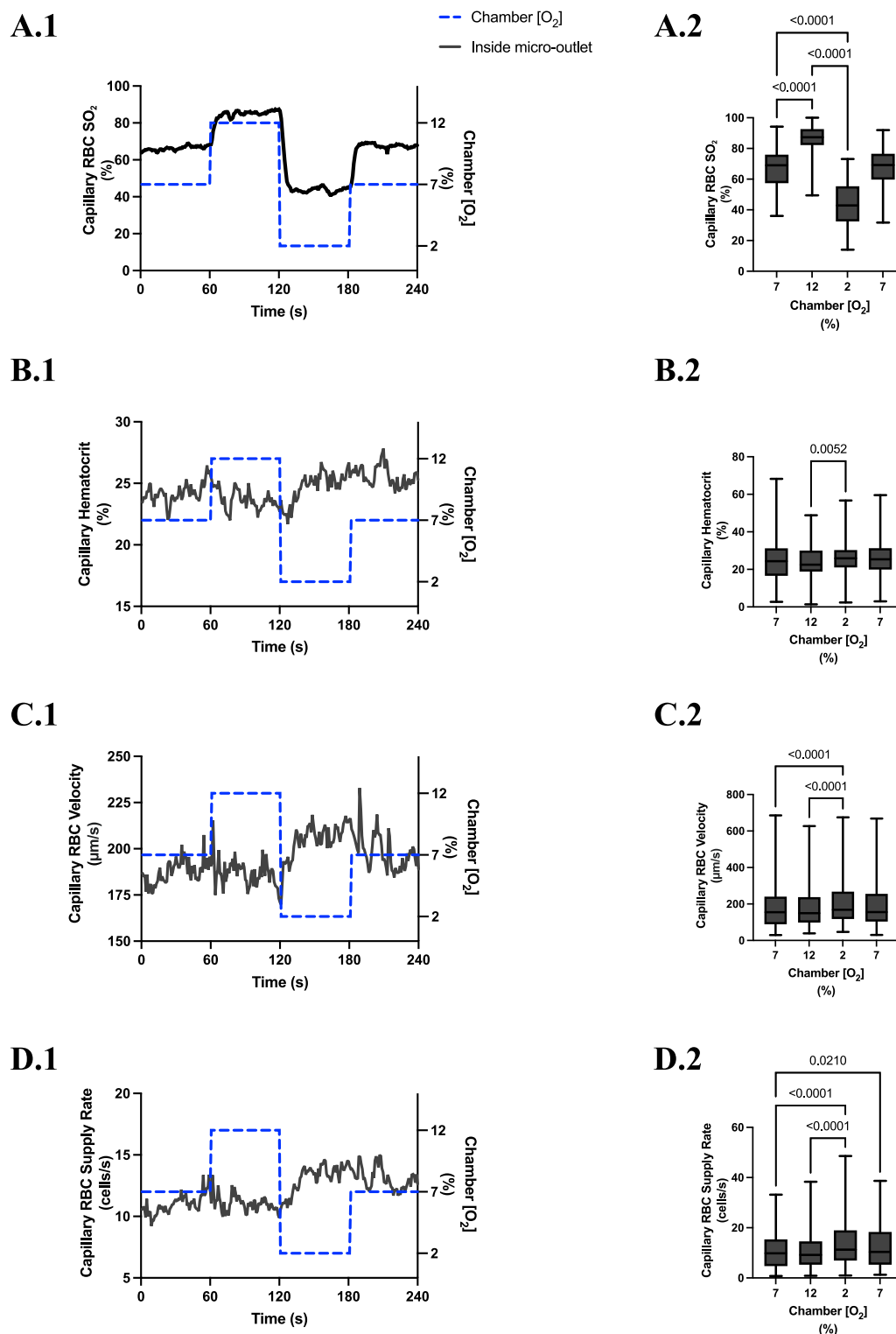


FIGURE 3

Capillary red blood cell (RBC) oxygen saturation (SO_2) and hemodynamic responses to oxygen concentration ($[O_2]$) oscillations for vessels directly overlying 400 μm micro-outlets. The micro-outlet gas exchange device imposed a 4-min $[O_2]$ oscillation consisting of 1-min $[O_2]$ perturbations at 7%, 12%, 2%, and 7%, respectively. Time series plots show the mean capillary RBC (SO_2) (A.1), hematocrit (B.1), velocity (C.1), and supply rate (D.1) in capillaries overlying the 400 μm micro-outlet edge across the 4-min $[O_2]$ oscillation (7% (1 min) \rightarrow 12% (1 min) \rightarrow 2% (1 min) \rightarrow 7% (1 min)). Comparisons between the baseline 7% period and the oscillation perturbations for capillary RBC SO_2 (A.2), hematocrit (B.2), velocity (C.2) and supply rate (D.2) were made using mean values taken from the entire first minute at baseline 7% $[O_2]$ and the last 15 s at 12%, 2%, and 7% ($n = 86$ capillaries). p values indicated in the figure with a $p < 0.05$ are considered significant. Box and whisker plots show minimum, median, maximum, and associated quartiles.

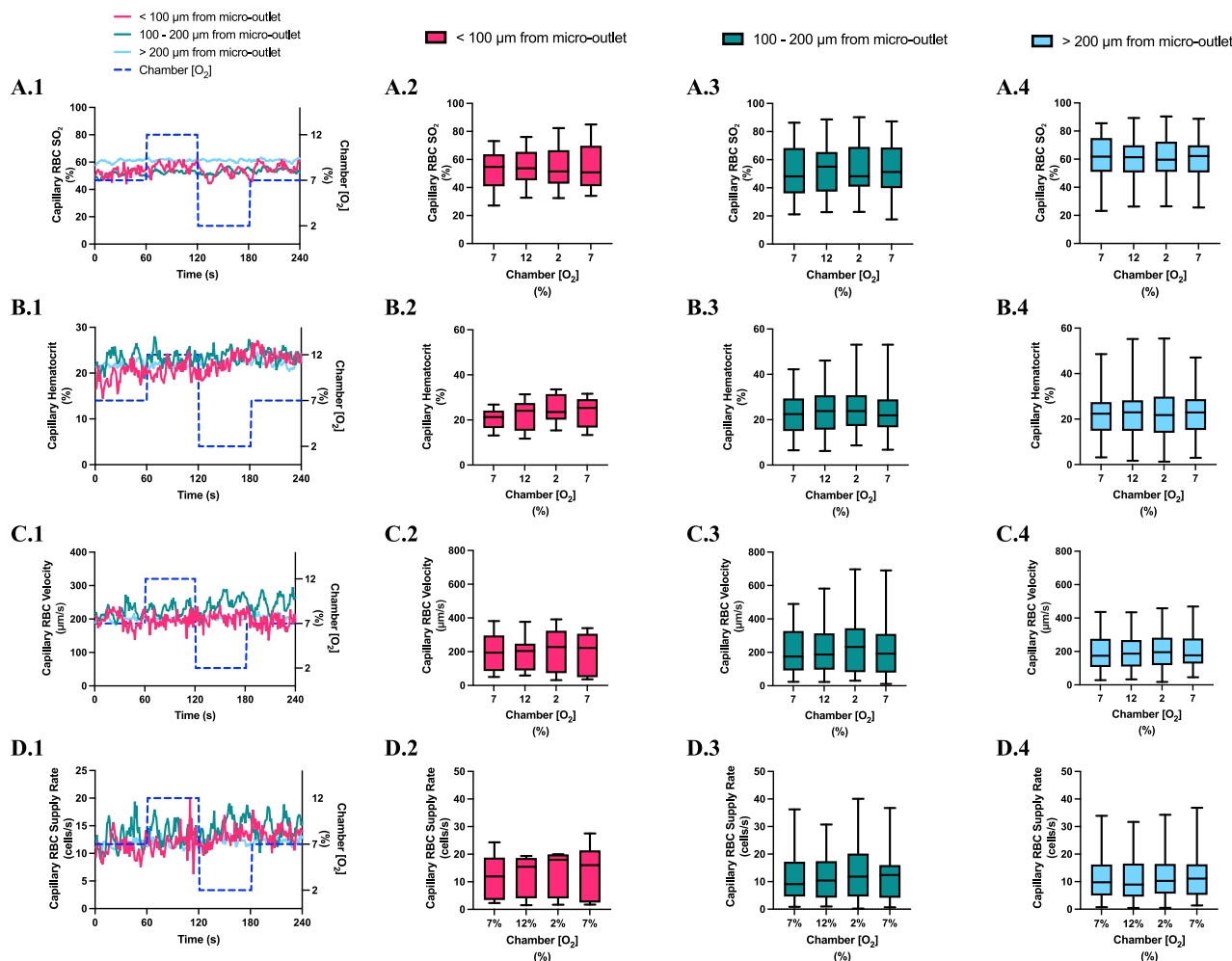


FIGURE 4

Capillary red blood cell (RBC) oxygen saturation (SO_2) and hemodynamic responses to oxygen concentration ($[\text{O}_2]$) oscillations for vessels at various distances outside the 400 μm micro-outlets. (A.1–D.1) represent time series plots for mean capillary RBC (SO_2), hematocrit, velocity, and supply rate, respectively for capillaries outside the micro-outlet edge at varying distances across the 4-min O_2 oscillations (7→12→2→7%). The micro-outlet gas exchange device imposed 4-min $[\text{O}_2]$ oscillations consisting of 1-min $[\text{O}_2]$ perturbations at 7%, 12%, 2%, and 7%, respectively. (A.2–A.4) represents mean capillary RBC SO_2 of capillaries within 100 μm from the micro-outlet edge ($n = 8$ capillaries), between 100–200 μm from the outlet edge ($n = 34$ capillaries), and greater than 200 μm from the outlet edge ($n = 71$ capillaries), respectively. (B.2–B.4) represents mean capillary hematocrit of capillaries within 100 μm from the micro-outlet edge ($n = 8$ capillaries), between 100–200 μm from the outlet edge ($n = 35$ capillaries), and greater than 200 μm from the outlet edge ($n = 73$ capillaries), respectively. (C.2–C.4) represents mean capillary RBC velocity of capillaries within 100 μm from the micro-outlet edge ($n = 8$ capillaries), between 100–200 μm from the outlet edge ($n = 35$ capillaries), and greater than 200 μm from the outlet edge ($n = 73$ capillaries), respectively. (D.2–D.4) represents mean capillary RBC supply rate of capillaries within 100 μm from the micro-outlet edge ($n = 8$ capillaries), between 100–200 μm from the outlet edge ($n = 35$ capillaries), and greater than 200 μm from the outlet edge ($n = 73$ capillaries), respectively. Box and whisker plots show minimum, median, maximum, and associated quartiles.

$218.6 \pm 189.0 \mu\text{m/s}$ ($p < 0.0001$) (Figure 7). Low $[\text{O}_2]$ challenges caused a significant increase in capillary RBC velocity in vessels between 100 and 200 μm away from the outlet edge at 2% GEC $[\text{O}_2]$, $385.9 \pm 237.4 \mu\text{m/s}$, compared to baseline 7% GEC $[\text{O}_2]$, $355.6 \pm 244.1 \mu\text{m/s}$ ($p = 0.0245$) (Figure 8). Vessels greater than 200 μm away from the outlet edge experienced significant changes in capillary RBC velocity at 2% GEC $[\text{O}_2]$, $282.0 \pm 178.9 \mu\text{m/s}$, compared to baseline 7% GEC $[\text{O}_2]$, $253.9 \pm 153.0 \mu\text{m/s}$ ($p = 0.0277$) (Figure 8).

High $[\text{O}_2]$ challenges imposed on capillaries directly overlying 400 μm micro-outlets caused significant changes in capillary RBC supply rate at 12% GEC $[\text{O}_2]$, $9.5 \pm 5.7 \text{ cells/s}$, compared to baseline

7% GEC $[\text{O}_2]$, $10.7 \pm 7.2 \text{ cells/s}$ ($p = 0.0232$) (Figure 5). Low $[\text{O}_2]$ challenges imposed on capillaries directly overlying 400 μm micro-outlets caused significant changes in capillary RBC supply rate at 2% GEC $[\text{O}_2]$, $17.7 \pm 13.4 \text{ cells/s}$, compared to baseline 7% GEC $[\text{O}_2]$, $10.7 \pm 8.1 \text{ cells/s}$ ($p < 0.0001$) (Figure 7). $[\text{O}_2]$ challenges imposed on capillaries directly overlying 400 μm micro-outlets caused significant changes in capillary RBC supply rate in vessels greater than 200 μm from the outlet edge at 2% GEC $[\text{O}_2]$, $18.4 \pm 12.2 \text{ cells/s}$, compared to a baseline 7% GEC $[\text{O}_2]$, $14.7 \pm 10.5 \text{ cells/s}$ ($p = 0.0004$) (Figure 8). No other outlet vessels had significant changes in capillary RBC supply rate during high and low $[\text{O}_2]$ challenges.

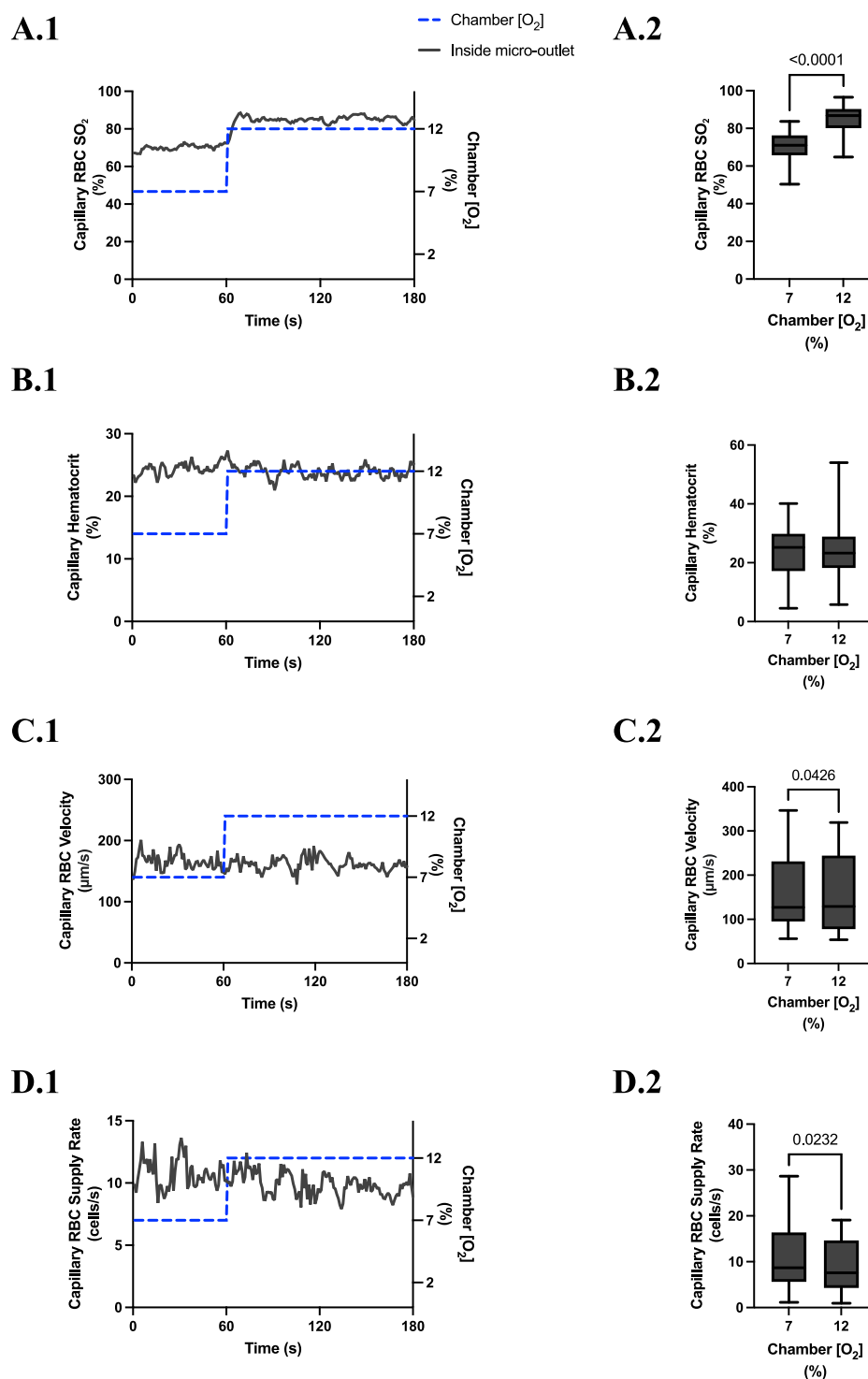
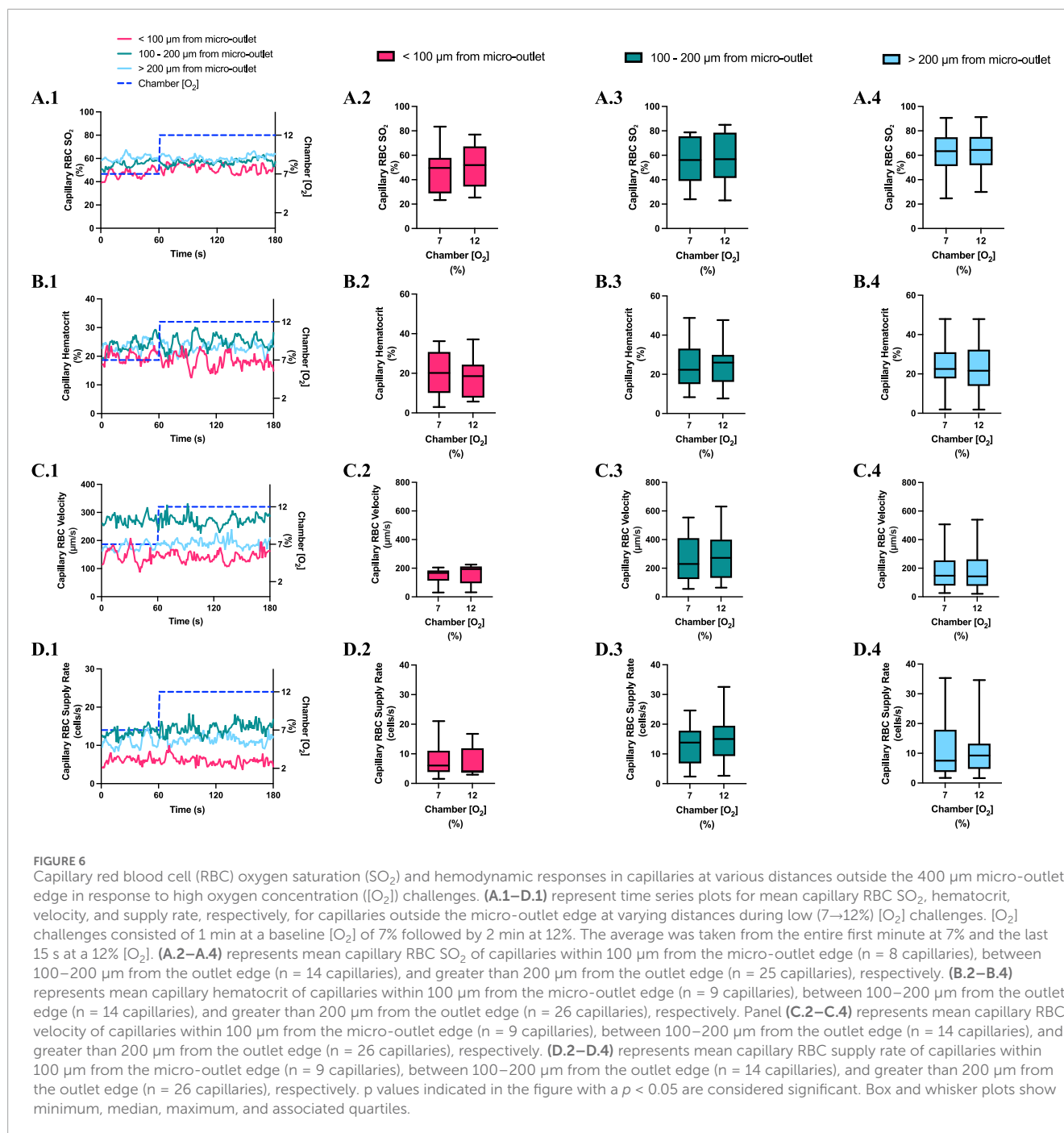


FIGURE 5

Capillary red blood cell (RBC) oxygen saturation (SO_2) and hemodynamic responses in capillaries directly overlying the 400 μm micro-outlet edge in response to high oxygen concentration ($[O_2]$) challenges. $[O_2]$ challenges began with 1-min baseline $[O_2]$ at 7% followed by 2 min at 12%. Time series plots are displayed in (A.1–D.1) for mean capillary RBC SO_2 (A.1), hematocrit (B.1), velocity (C.1), and supply rate (D.1), for capillaries overlying the micro-outlet during low $[O_2]$ challenges. For (A.2–D.2), the average was taken from the entire first minute at 7% and the last 15 s at 12% $[O_2]$. (A.2–D.2) represent mean RBC SO_2 ($n = 28$ capillaries), hematocrit, velocity, and supply rate ($n = 28$ capillaries), respectively, for capillaries directly overlying the 200 μm micro-outlet. p values indicated in the figure with a $p < 0.05$ are considered significant. Box and whisker plots show minimum, median, maximum, and associated quartiles.



Computer simulation results showing the steady state PO_2 within the tissue and micro-outlet device for high (12%) and low (2%) $[\text{O}_2]$ challenges are presented in Figure 9. Simulations predict that the volume perturbed by the 400 μm diameter micro-outlet are highly constrained to the tissue region directly overlying the micro-outlet-to-tissue interface. Importantly, the model predicts that the PVDC barrier layer in the micro-outlet device presents considerable resistance to oxygen diffusion, effectively constraining gas flux to the PDMS surface of the micro-outlet. Simulations of steady state conditions while the gas exchange chamber $[\text{O}_2]$ is held at 2% predicted that PO_2 within the tissue volume would be decreased

by >2 mmHg up to a radial distance of 17.0 μm beyond the micro-outlet edge, and up to 61.0 μm vertically into the tissue volume in the Z-axis along the center of the circular micro-outlet. At 2% $[\text{O}_2]$, tissue PO_2 at the center of the micro-outlet-tissue interface was predicted to be 29.9 mmHg, and 30.8 mmHg directly above the micro-outlet 10 μm into the tissue volume (Figure 9). Simulations for high (12%) $[\text{O}_2]$ within the GEC predicted an increase in tissue PO_2 of >2 mmHg up to a radial distance of 59.0 μm beyond the micro-outlet edge, and a depth into the tissue volume up to 125.0 μm (Figure 9). At 12% $[\text{O}_2]$, tissue PO_2 at the center of the micro-outlet-tissue interface was predicted to be 52.7 mmHg, and 50.3 mmHg

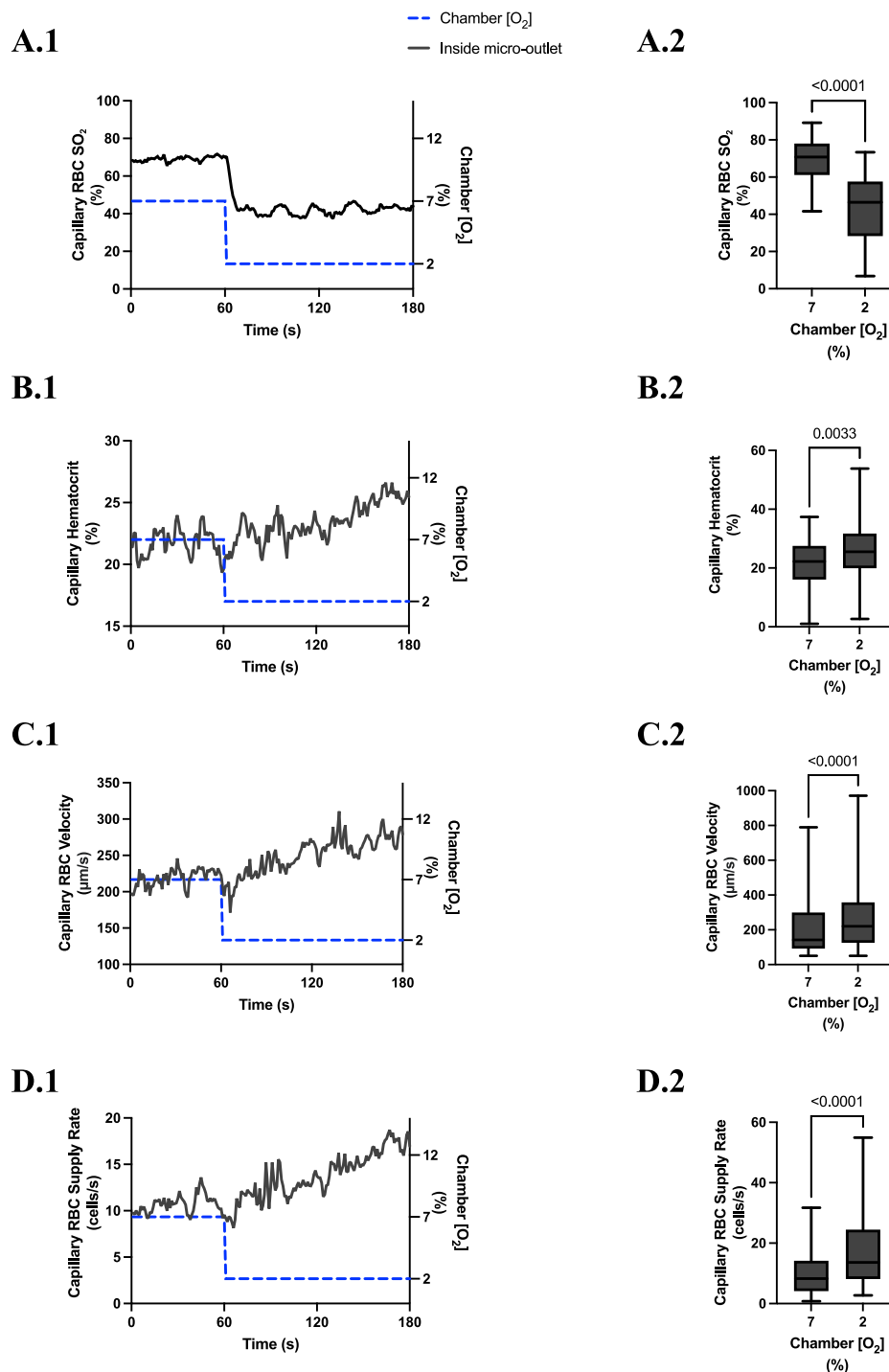


FIGURE 7

Capillary red blood cell (RBC) oxygen saturation (SO_2) and hemodynamic responses in capillaries directly overlying the 400 μm micro-outlet edge in response to low oxygen concentration ($[O_2]$) challenges. $[O_2]$ challenges began with 1-min baseline $[O_2]$ at 7% followed by 2 min at 2%. Time series plots are displayed in (A.1–D.1) for mean capillary RBC SO_2 (A.1), hematocrit (B.1), velocity (C.1), and supply rate (D.1), for capillaries overlying the micro-outlet during low $[O_2]$ challenges. For (A.2–D.2), the average was taken from the entire first minute at 7% and the last 15 s at 2% $[O_2]$. (A.2–D.2) represent mean RBC SO_2 ($n = 36$ capillaries), hematocrit, velocity, and supply rate ($n = 36$ capillaries), respectively, for capillaries directly overlying the 400 μm micro-outlet. p values indicated in the figure with a $p < 0.05$ are considered significant. Box and whisker plots show minimum, median, maximum, and associated quartiles.

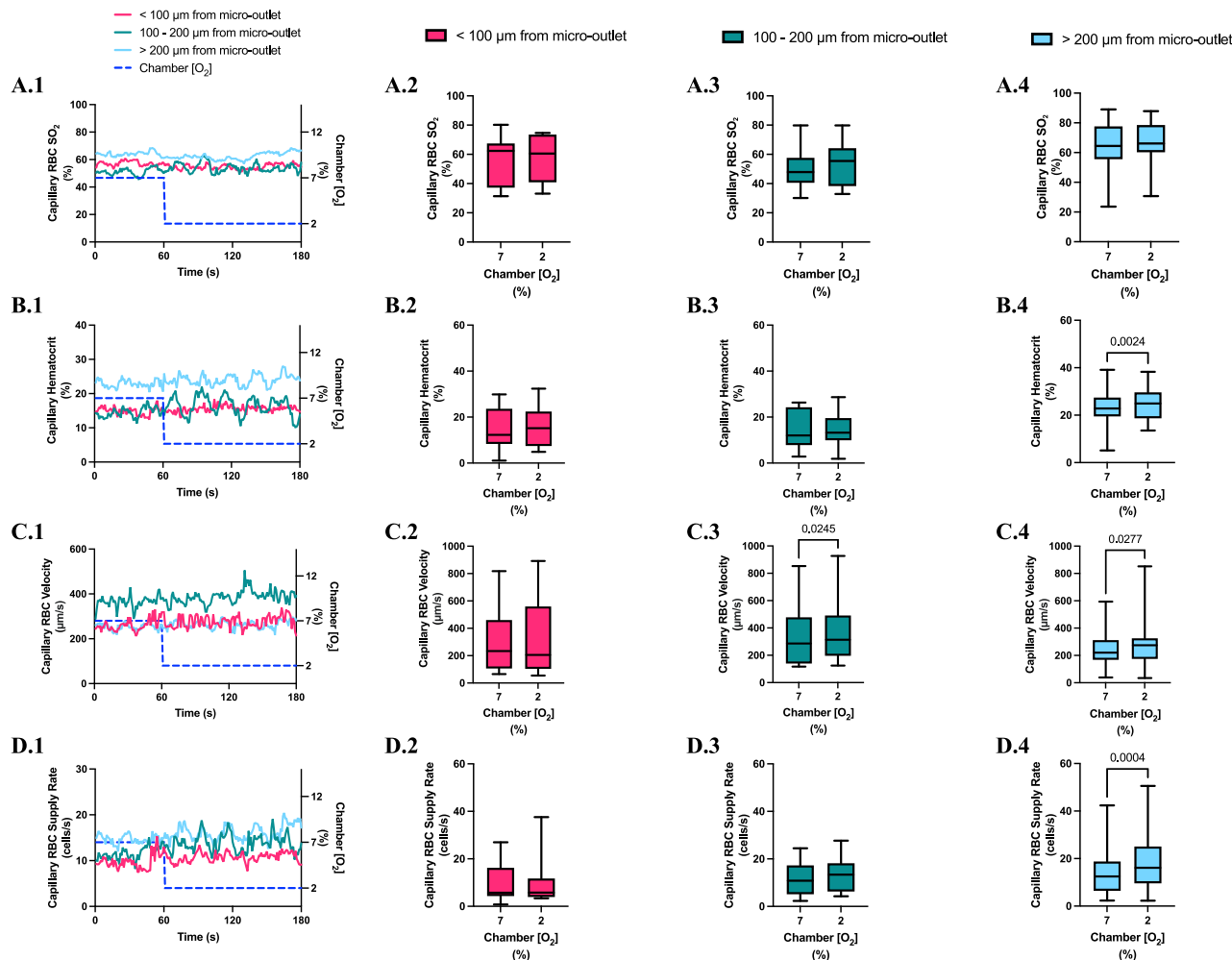


FIGURE 8

Capillary red blood cell (RBC) oxygen saturation (SO_2) and hemodynamic responses in capillaries at various distances outside the 400 μm micro-outlet edge in response to low oxygen concentration ($[O_2]$) challenges. (A.1–D.1) represent time series plots for mean capillary RBC SO_2 , hematocrit, velocity, and supply rate, respectively, for capillaries outside the micro-outlet edge at varying distances during low (7→2%) $[O_2]$ challenges. $[O_2]$ challenges consisted of 1 min at a baseline $[O_2]$ of 7% followed by 2 min at 2%. The average was taken from the entire first minute at 7% and the last 15 s at a 2% $[O_2]$. (A.2–A.4) represents mean capillary RBC SO_2 of capillaries within 100 μm from the micro-outlet edge ($n = 7$ capillaries), between 100–200 μm from the outlet edge ($n = 11$ capillaries), and greater than 200 μm from the outlet edge ($n = 17$ capillaries), respectively. (B.2–B.4) represents mean capillary hematocrit of capillaries within 100 μm from the micro-outlet edge ($n = 15$ capillaries), between 100–200 μm from the outlet edge ($n = 14$ capillaries), and greater than 200 μm from the outlet edge ($n = 23$ capillaries), respectively. (C.2–C.4) represents mean capillary RBC velocity of capillaries within 100 μm from the micro-outlet edge ($n = 15$ capillaries), between 100–200 μm from the outlet edge ($n = 14$ capillaries), and greater than 200 μm from the outlet edge ($n = 23$ capillaries), respectively. (D.2–D.4) represents mean capillary RBC supply rate of capillaries within 100 μm from the micro-outlet edge ($n = 15$ capillaries), between 100–200 μm from the outlet edge ($n = 14$ capillaries), and greater than 200 μm from the outlet edge ($n = 23$ capillaries), respectively. p values indicated in the figure with a $p < 0.05$ are considered significant. Box and whisker plots show minimum, median, maximum, and associated quartiles.

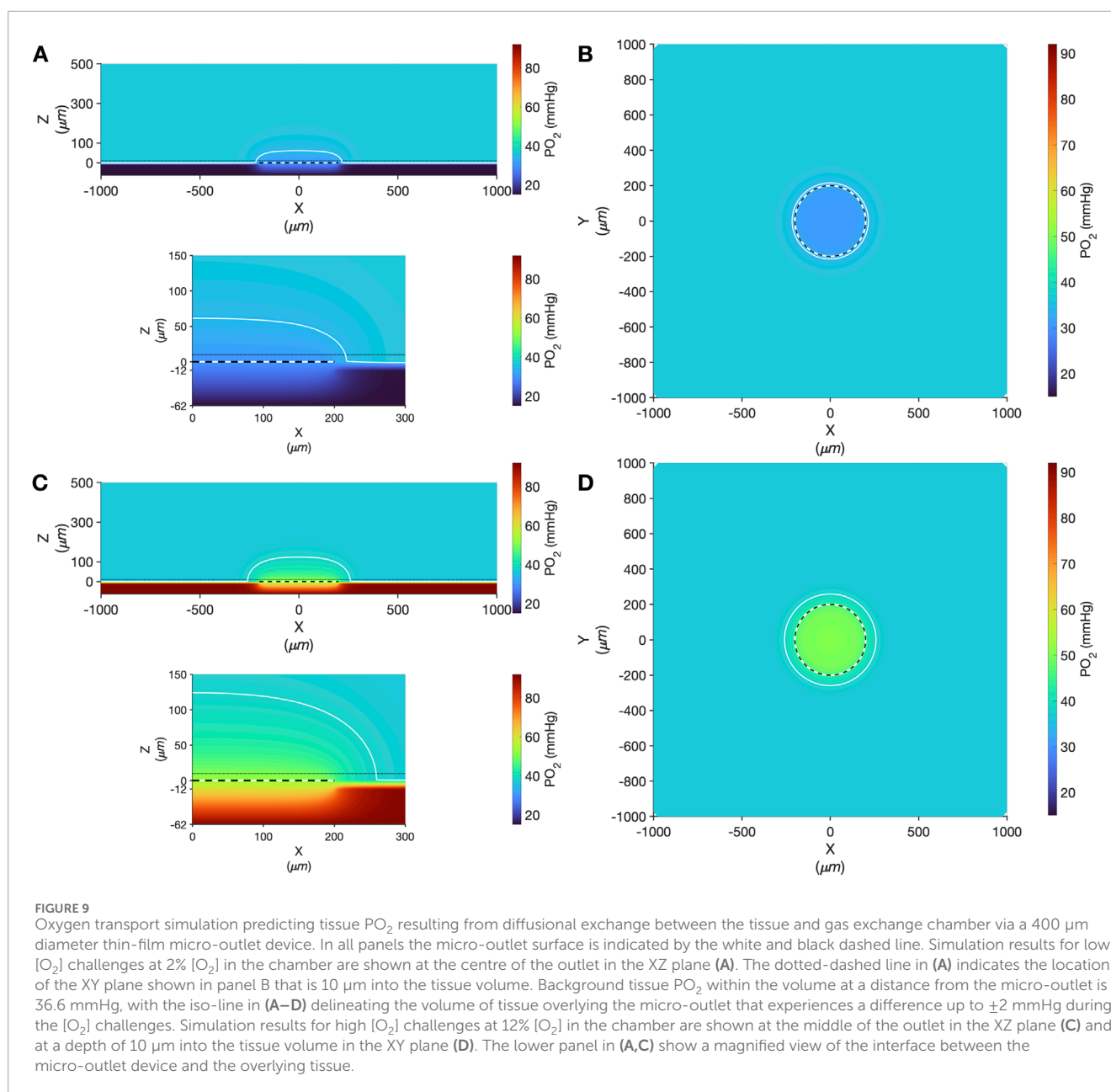
directly above the micro-outlet 10 μm into the tissue volume (Figure 9).

3.5 200 μm micro-outlet oxygen challenge data

High $[O_2]$ challenges imposed on capillaries directly overlying 200 μm micro-outlets caused significant elevation in capillary RBC SO_2 at 12% GEC $[O_2]$, $81.3\% \pm 13.0\%$, compared to baseline 7% GEC $[O_2]$, $60.6\% \pm 16.9\%$ ($p < 0.0001$) (Figure 10). Low $[O_2]$

challenges imposed on capillaries directly overlying 200 μm micro-outlets caused significant decrease in capillary RBC SO_2 at 2% GEC $[O_2]$, $43.7\% \pm 18.7\%$, compared to baseline 7% GEC $[O_2]$, $65.3\% \pm 13.0\%$ ($p < 0.0001$) (Figure 13).

High $[O_2]$ challenges imposed on capillaries directly overlying 200 μm micro-outlets caused significant increase in capillary RBC SO_2 at 12% GEC $[O_2]$, $49.2\% \pm 15.6\%$, compared to baseline 7% GEC $[O_2]$, $44.5\% \pm 15.4\%$ in capillaries less than 100 μm away from the outlet edge ($p = 0.0009$) (Figure 11). There were no significant increases or decreases in capillary RBC SO_2 at 2% GEC $[O_2]$, compared to baseline 7% GEC



$[O_2]$, in capillaries outside the micro-outlet at any distance from edge (Figure 12).

High $[O_2]$ challenges imposed on capillaries directly overlying 200 μm micro-outlets caused a small but significant increase in capillary hematocrit in vessels greater than 200 μm away from the outlet at 12% GEC $[O_2]$, $20.1\% \pm 9.6\%$, compared to baseline 7% GEC $[O_2]$, $19.1\% \pm 9.5\%$ ($p = 0.0172$) (Figure 11). $[O_2]$ challenges imposed on capillaries directly overlying 200 μm micro-outlets caused significant changes in capillary hematocrit at 2% GEC $[O_2]$, $22.9\% \pm 10.2\%$, compared to baseline 7% GEC $[O_2]$, $20.7\% \pm 8.5\%$ ($p = 0.0022$) (Figure 12). $[O_2]$ challenges imposed on capillaries directly overlying 200 μm micro-outlets caused a significant increase in capillary hematocrit in vessels less than 100 μm away from the outlet at 2% GEC $[O_2]$, $18.9\% \pm 10.7\%$, compared to baseline 7% GEC $[O_2]$, $17.8\% \pm 10.4\%$ ($p = 0.0348$) (Figure 13).

$[O_2]$ challenges imposed on capillaries directly overlying 200 μm micro-outlets caused significant changes in capillary RBC velocity at 12% GEC $[O_2]$, $192.7 \pm 107.5 \mu m/s$, compared to baseline 7% GEC $[O_2]$, $207.5 \pm 123.7 \mu m/s$ ($p = 0.0370$) (Figure 10). $[O_2]$ challenges imposed on capillaries directly overlying 200 μm micro-outlets caused significant changes in capillary RBC velocity at 2% GEC $[O_2]$, $293.1 \pm 175.6 \mu m/s$, compared to baseline 7% GEC $[O_2]$, $230.2 \pm 141.0 \mu m/s$ ($p < 0.0001$) (Figure 12).

$[O_2]$ challenges imposed on 200 μm micro-outlets caused significant changes in capillary RBC velocity in vessels greater than 200 μm away from the outlet at 12% GEC $[O_2]$, $197.2 \pm 117.8 \mu m/s$ compared to baseline 7% GEC $[O_2]$, $183.5 \pm 116.5 \mu m/s$ ($p = 0.0211$) (Figure 11). $[O_2]$ challenges imposed on 200 μm micro-outlets caused a significant increase in capillary RBC velocity in vessels less than 100 μm away from the outlet at 2% GEC $[O_2]$,

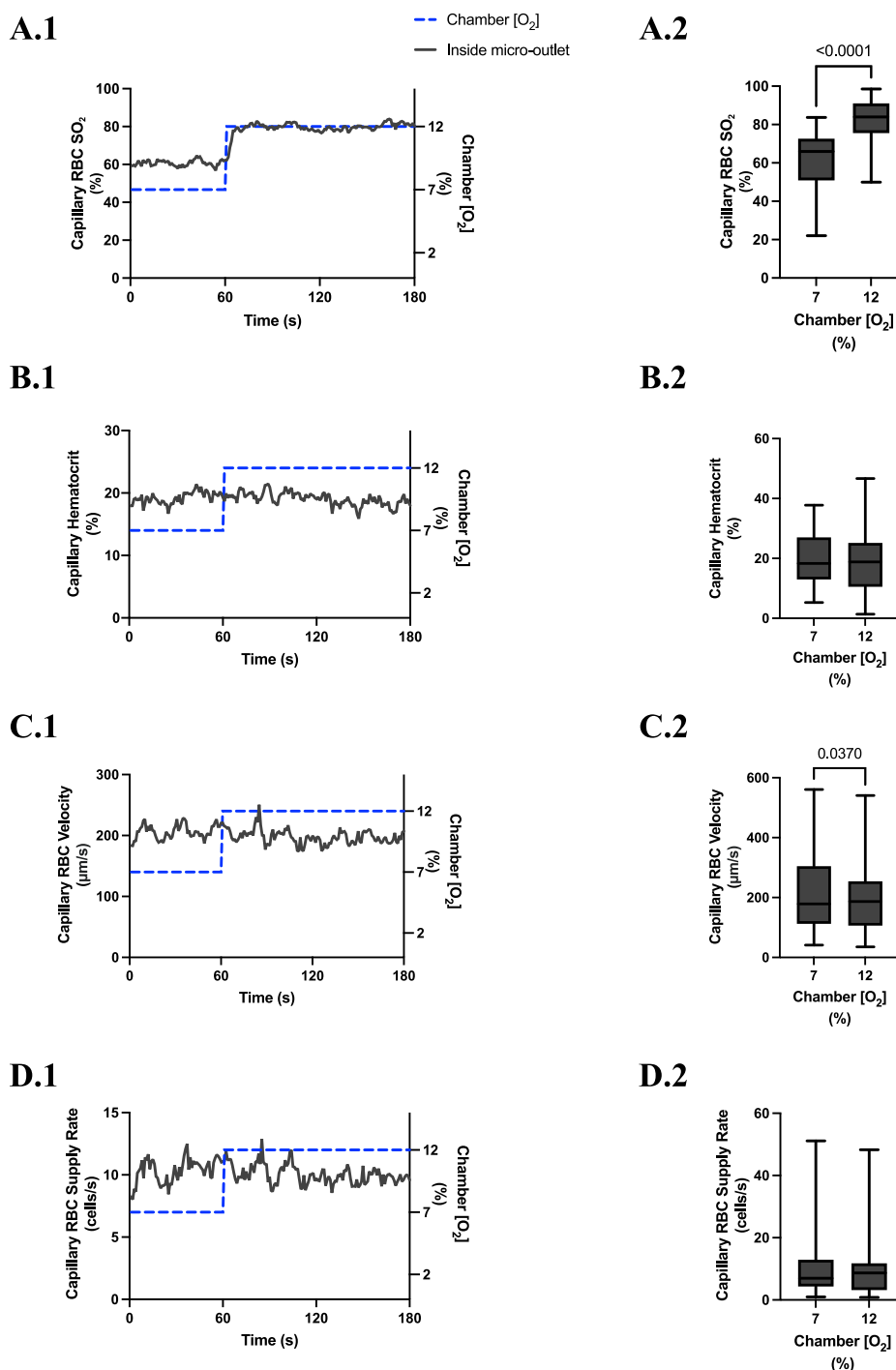


FIGURE 10

Capillary red blood cell (RBC) oxygen saturation (SO_2) and hemodynamic responses in capillaries directly overlying the 200 μm micro-outlet edge in response to high oxygen concentration ($[\text{O}_2]$) challenges. $[\text{O}_2]$ challenges began with 1-min baseline $[\text{O}_2]$ at 7% followed by 2 min at 12%. Time series plots are displayed in (A.1–D.1) for mean capillary RBC SO_2 (A.1), hematocrit (B.1), velocity (C.1), and supply rate (D.1), for capillaries overlying the micro-outlet during low $[\text{O}_2]$ challenges. For (A.2–D.2), the average was taken from the entire first minute at 7% and the last 15 s at 12% $[\text{O}_2]$. (A.2–D.2) represent mean RBC SO_2 ($n = 44$ capillaries), hematocrit, velocity, and supply rate ($n = 42$ capillaries), respectively, for capillaries directly overlying the 200 μm micro-outlet. p values indicated in the figure with a $p < 0.05$ are considered significant. Box and whisker plots show minimum, median, maximum, and associated quartiles.

$207.8 \pm 123.6 \mu\text{m/s}$ compared to baseline 7% GEC $[\text{O}_2]$, $182.0 \pm 118.9 \mu\text{m/s}$, in vessels between 100–200 μm away at 2% GEC $[\text{O}_2]$, $223.8 \pm 122.3 \mu\text{m/s}$, compared to baseline 7% GEC $[\text{O}_2]$, $189.1 \pm$

$95.1 \mu\text{m/s}$, and in vessels greater than 200 μm away from the outlet at 2% GEC $[\text{O}_2]$, $225.9 \pm 143.8 \mu\text{m/s}$ compared to baseline 7% GEC $[\text{O}_2]$, $210.1 \pm 119.8 \mu\text{m/s}$ ($p < 0.0161$) (Figure 13).

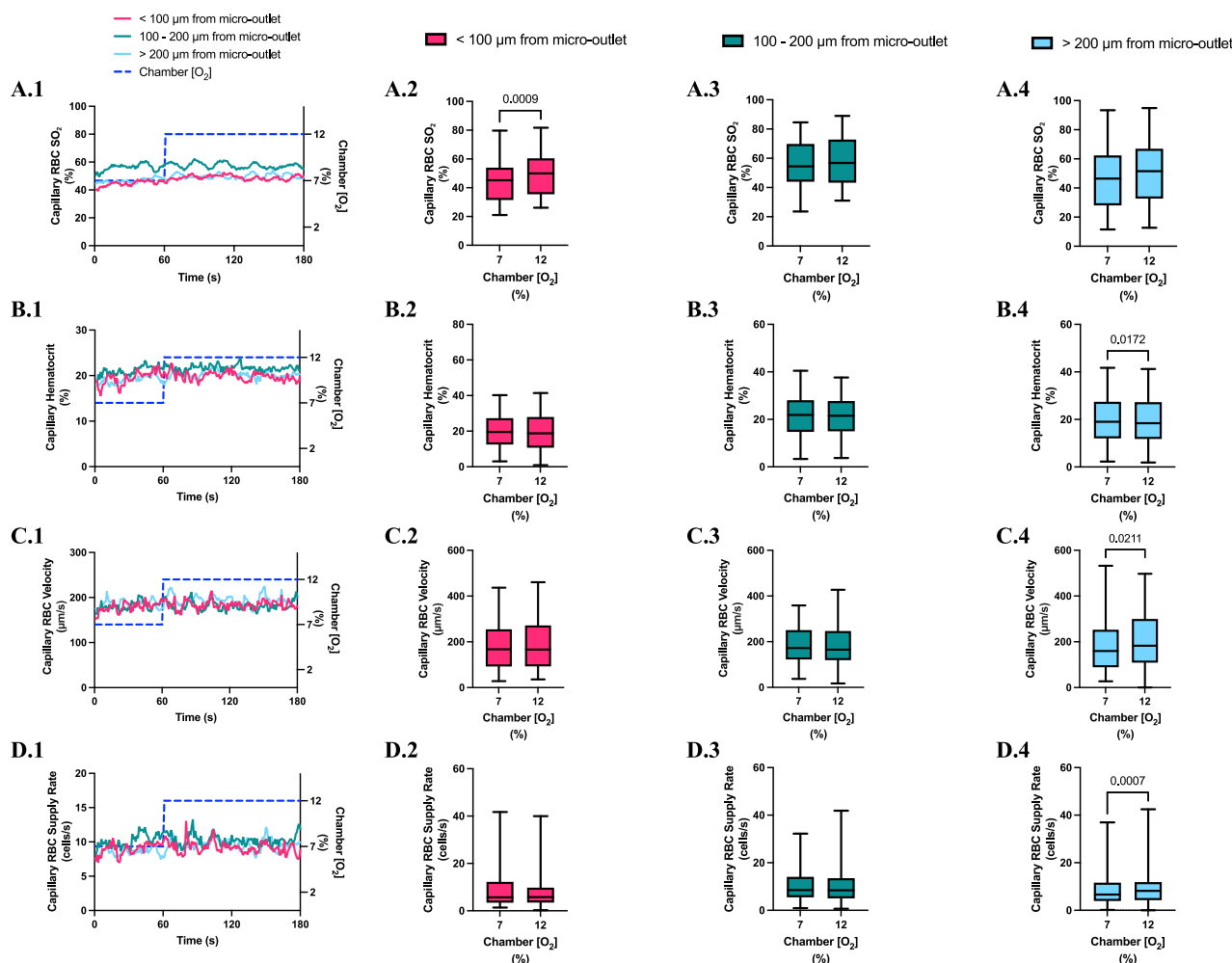


FIGURE 11

Capillary red blood cell (RBC) oxygen saturation (SO_2) and hemodynamic responses in capillaries at various distances outside the 200 μm micro-outlet edge in response to high oxygen concentration ($[O_2]$) challenges. (A.1–D.1) represent time series plots for mean capillary RBC SO_2 , hematocrit, velocity, and supply rate, respectively, for capillaries outside the micro-outlet edge at varying distances during high (7→12%) $[O_2]$ challenges. $[O_2]$ challenges consisted of 1 min at a baseline $[O_2]$ of 7% followed by 2 min at 12%. Means were calculated from the entire first minute at 7% and the last 15 s at a 12% $[O_2]$. (A.2–A.4) represents mean capillary RBC SO_2 of capillaries within 100 μm from the micro-outlet edge ($n = 37$ capillaries), between 100–200 μm from the outlet edge ($n = 38$ capillaries), and greater than 200 μm from the outlet edge ($n = 48$ capillaries), respectively. (B.2–B.4) represents mean capillary hematocrit of capillaries within 100 μm from the micro-outlet edge ($n = 31$ capillaries), between 100–200 μm from the outlet edge ($n = 54$ capillaries), and greater than 200 μm from the outlet edge ($n = 68$ capillaries), respectively. (C.2–C.4) represents mean capillary RBC velocity of capillaries within 100 μm from the micro-outlet edge ($n = 31$ capillaries), between 100–200 μm from the outlet edge ($n = 54$ capillaries), and greater than 200 μm from the outlet edge ($n = 68$ capillaries), respectively. (D.2–D.4) represents mean capillary RBC supply rate of capillaries within 100 μm from the micro-outlet edge ($n = 31$ capillaries), between 100–200 μm from the outlet edge ($n = 54$ capillaries), and greater than 200 μm from the outlet edge ($n = 68$ capillaries), respectively. p values indicated in the figure with a $p < 0.05$ are considered significant. Box and whisker plots show minimum, median, maximum, and associated quartiles.

$[O_2]$ challenges imposed on capillaries directly overlying 200 μm micro-outlets caused a significant increase in capillary RBC supply rate at 2% GEC $[O_2]$, 17.3 ± 12.3 cells/s, compared to baseline 7% GEC $[O_2]$, 12.6 ± 10.2 cells/s ($p < 0.0001$) but not at 12% GEC $[O_2]$ (Figures 10, 12). $[O_2]$ challenges imposed on 200 μm micro-outlets caused significant changes in capillary RBC supply rate for vessels 200 μm away from the outlet edge at 12% GEC $[O_2]$, 9.6 ± 7.8 cells/s, compared to baseline 7% GEC $[O_2]$, 8.5 ± 6.9 cells/s ($p = 0.0007$) (Figure 11). $[O_2]$ challenges imposed on capillaries directly overlying 200 μm micro-outlets caused a significant increase in capillary RBC supply rate for vessels less than 100 μm away at 2%

GEC $[O_2]$, 11.0 ± 9.3 cells/s, compared to baseline 7% GEC $[O_2]$, 9.0 ± 8.7 cells/s, in vessels in the 100–200 μm range from the outlet edge at 2% GEC $[O_2]$, 12.2 ± 8.7 cells/s, compared to baseline 7% GEC $[O_2]$, 9.1 ± 6.8 cells/s, and in vessels greater than 200 μm away at 2% GEC $[O_2]$, 11.2 ± 11.3 cells/s compared to baseline 7% GEC $[O_2]$, 9.5 ± 8.7 cells/s ($p < 0.0248$) (Figure 13).

Computer simulation results showing the steady state PO_2 within the tissue and 200 μm micro-outlet device for high (12%) and low (2%) $[O_2]$ challenges are presented in Figure 14. Simulations of steady state conditions while the gas exchange chamber $[O_2]$ is held at 2% predicted that PO_2 within the tissue volume would

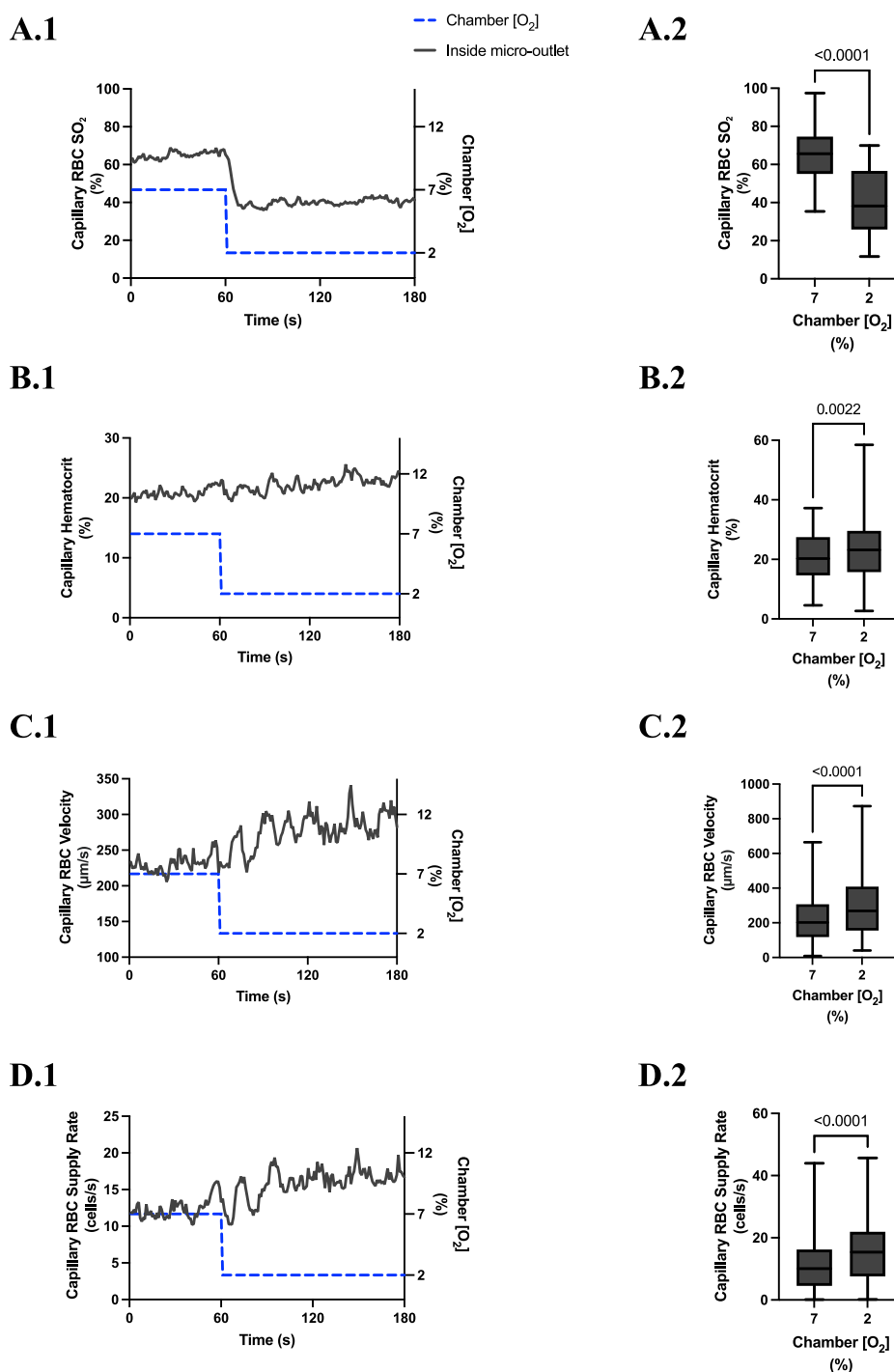


FIGURE 12

Capillary red blood cell (RBC) oxygen saturation (SO_2) and hemodynamic responses in capillaries directly overlying the 200 μm micro-outlet edge in response to low oxygen concentration ($[O_2]$) challenges. $[O_2]$ challenges began with 1-min baseline $[O_2]$ at 7% followed by 2 min at 2%. Time series plots are displayed in (A.1–D.1) for mean capillary RBC SO_2 (A.1), hematocrit (B.1), velocity (C.1), and supply rate (D.1), for capillaries overlying the micro-outlet during low $[O_2]$ challenges. For (A.2–D.2), the average was taken from the entire first minute at 7% and the last 15 s at 2% $[O_2]$. (A.2–D.2) represent mean RBC SO_2 ($n = 43$ capillaries), hematocrit, velocity, and supply rate ($n = 53$ capillaries), respectively, for capillaries directly overlying the 200 μm micro-outlet. p values indicated in the figure with a $p < 0.05$ are considered significant. Box and whisker plots show minimum, median, maximum, and associated quartiles.

be decreased by >2 mmHg up to a radial distance of 16.5 μm beyond the micro-outlet edge, and up to 54.5 μm vertically into the tissue volume in the Z-axis along the centre of the circular

micro-outlet (Figure 14). Simulations for high (12%) $[O_2]$ within the gas exchange chamber predicted an increase in tissue PO_2 of >2 mmHg up to a radial distance of 49.5 μm beyond the micro-

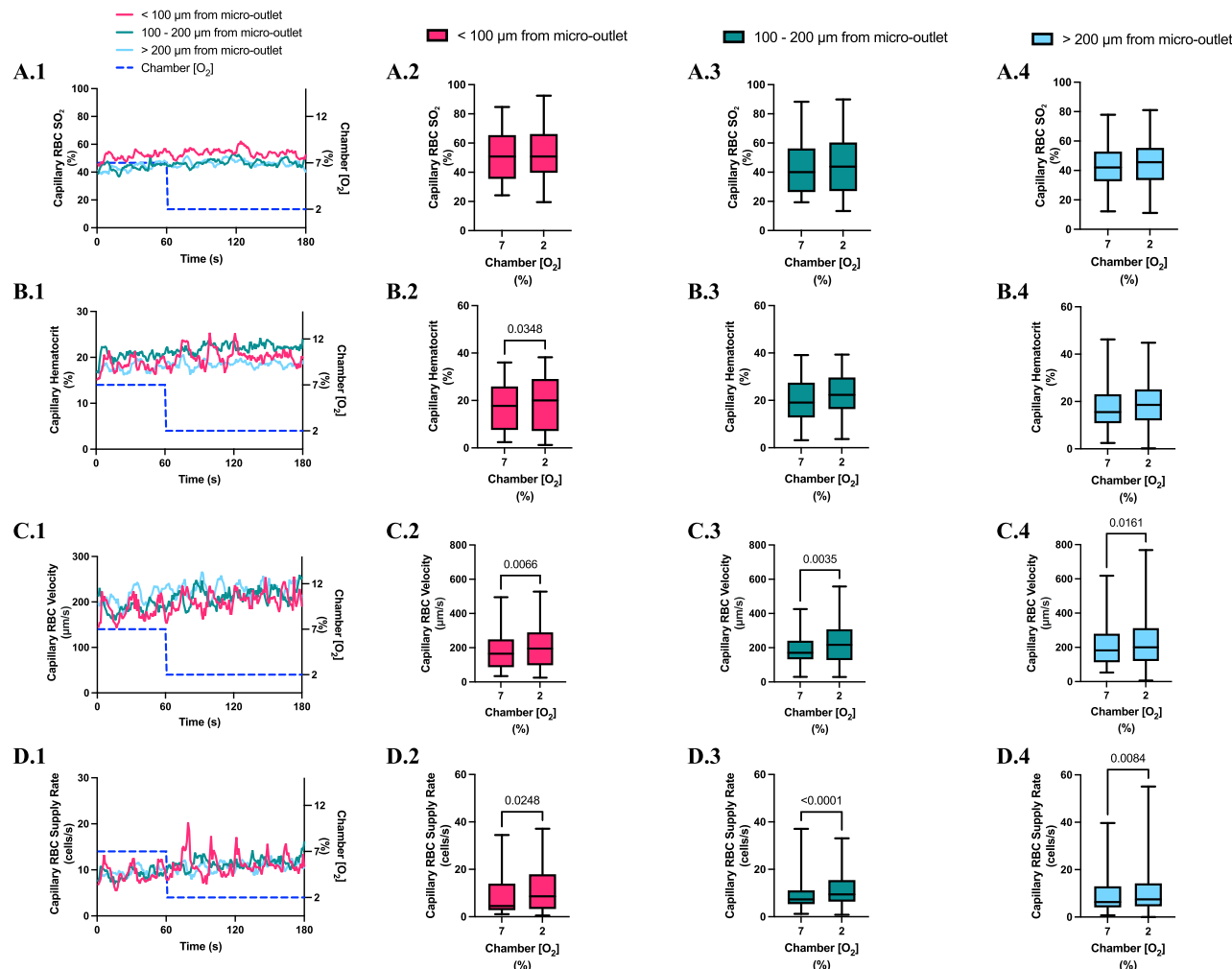


FIGURE 13
Capillary red blood cell (RBC) oxygen saturation (SO_2) and hemodynamic responses in capillaries at various distances outside the 200 μm micro-outlet edge in response to low oxygen concentration ($[\text{O}_2]$) challenges. (A.1–D.1) represent time series plots for mean capillary RBC SO_2 , hematocrit, velocity, and supply rate, respectively, for capillaries outside the micro-outlet edge at varying distances during low (7→2%) $[\text{O}_2]$ challenges. $[\text{O}_2]$ challenges consisted of 1 min at a baseline $[\text{O}_2]$ of 7% followed by 2 min at 2%. The average was taken from the entire first minute at 7% and the last 15 s at a 2% $[\text{O}_2]$. (A.2–A.4) represents mean capillary RBC SO_2 of capillaries within 100 μm from the micro-outlet edge ($n = 41$ capillaries), between 100–200 μm from the outlet edge ($n = 34$ capillaries), and greater than 200 μm from the outlet edge ($n = 57$ capillaries), respectively. (B.2–B.4) represents mean capillary hematocrit of capillaries within 100 μm from the micro-outlet edge ($n = 30$ capillaries), between 100–200 μm from the outlet edge ($n = 38$ capillaries), and greater than 200 μm from the outlet edge ($n = 72$ capillaries), respectively. (C.2–C.4) represents mean capillary RBC velocity of capillaries within 100 μm from the micro-outlet edge ($n = 30$ capillaries), between 100–200 μm from the outlet edge ($n = 38$ capillaries), and greater than 200 μm from the outlet edge ($n = 72$ capillaries), respectively. (D.2–D.4) represents mean capillary RBC supply rate of capillaries within 100 μm from the micro-outlet edge ($n = 30$ capillaries), between 100–200 μm from the outlet edge ($n = 38$ capillaries), and greater than 200 μm from the outlet edge ($n = 72$ capillaries), respectively. p values indicated in the figure with a $p < 0.05$ are considered significant. Box and whisker plots show minimum, median, maximum, and associated quartiles.

outlet edge, and a depth into the tissue volume up to 101.5 μm (Figure 14).

3.6 600 and 1,000 μm micro-outlet data

$[\text{O}_2]$ oscillations and challenges were also imposed using 600 and 1,000 μm micro-outlet devices to study how larger exchange surfaces may impact the resulting microhemodynamic responses. The data from these larger micro-outlet devices is largely comparable to the findings presented above for 200 and 400 μm micro-outlets.

To provide additional context we briefly discuss the responses to low (2%) $[\text{O}_2]$ challenges in the 600 and 1,000 μm micro-outlets devices below.

Low $[\text{O}_2]$ challenges imposed using 600 μm micro-outlets caused a significant decrease in capillary RBC SO_2 at 2% GEC $[\text{O}_2]$, $50.2\% \pm 18.33\%$, compared to baseline 7% GEC $[\text{O}_2]$, $72.4\% \pm 11.3\%$ ($p < 0.0001$) (Supplementary Figure S3). Low $[\text{O}_2]$ challenges caused significant increases in capillary hematocrit at 2% GEC $[\text{O}_2]$, $25.54\% \pm 10.82\%$, compared to baseline 7% GEC $[\text{O}_2]$, $21.36\% \pm 10.93\%$ ($p < 0.0001$); capillary RBC velocity at 2% GEC $[\text{O}_2]$, $291.1 \pm 182.7 \mu\text{m/s}$, compared to baseline 7% GEC $[\text{O}_2]$, $218.1 \pm$

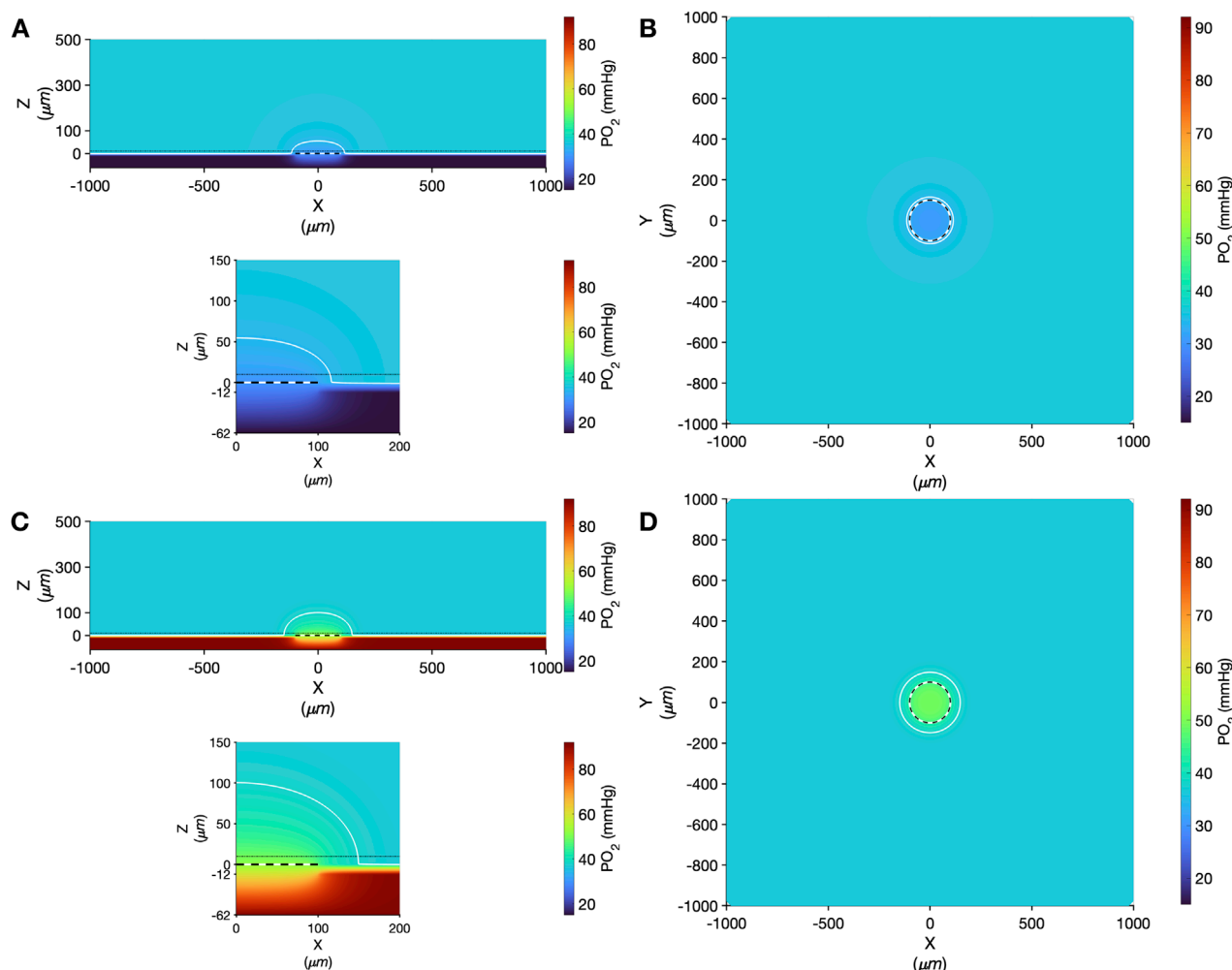


FIGURE 14

Oxygen transport simulation predicting tissue PO_2 resulting from diffusional exchange between the tissue and gas exchange chamber via a 200 μm diameter thin-film micro-outlet device. In all panels the micro-outlet surface is indicated by the white and black dashed line. Simulation results for low $[O_2]$ challenges at 2% $[O_2]$ in the chamber are shown at the centre of the outlet in the XZ plane (A). The dotted-dashed line in (A) indicates the location of the XY plane shown in panel B that is 10 μm into the tissue volume. Background tissue PO_2 within the volume at a distance from the micro-outlet is 36.6 mmHg, with the iso-line in (A–D) delineating the volume of tissue overlying the micro-outlet that experiences a difference up to ± 2 mmHg during the $[O_2]$ challenges. Simulation results for high $[O_2]$ challenges at 12% $[O_2]$ in the chamber are shown at the middle of the outlet in the XZ plane (C) and at a depth of 10 μm into the tissue volume in the XY plane (D). The lower panel in A and C show a magnified view of the interface between the micro-outlet device and the overlying tissue.

149.4 $\mu m/s$ ($p < 0.0001$); and supply rate at 2% GEC $[O_2]$, 18.4 ± 14.8 cells/s, compared to baseline 7% GEC $[O_2]$, 12.3 ± 11.9 cells/s ($p < 0.0001$) (Supplementary Figure S3).

Computer simulation results showing the steady state PO_2 within the tissue and 600 μm micro-outlet device for high (12%) and low (2%) $[O_2]$ challenges are presented in Supplementary Figure S4. Simulations of steady state conditions while the gas exchange chamber $[O_2]$ is held at 2% predicted that PO_2 within the tissue volume would be decreased by >2 mmHg up to a radial distance of 16.5 μm beyond the micro-outlet edge, and up to 61.4 μm vertically into the tissue volume in the Z-axis along the center of the circular micro-outlet (Supplementary Figure S4). Simulations for high (12%) $[O_2]$ within the gas exchange chamber predicted an increase in tissue PO_2

of >2 mmHg up to a radial distance of 64.5 μm beyond the micro-outlet edge, and a depth into the tissue volume up to 131.7 μm (Supplementary Figure S4).

Low $[O_2]$ challenges imposed using 1,000 μm micro-outlets caused significant decrease in capillary RBC SO_2 at 2% GEC $[O_2]$, $45.73\% \pm 19.75\%$, compared to baseline 7% GEC $[O_2]$, $71.15\% \pm 15.28\%$ ($p < 0.0001$) (Supplementary Figure S5). Low $[O_2]$ challenges caused significant increases in capillary hematocrit at 2% GEC $[O_2]$, $25.81\% \pm 9.12\%$, compared to baseline 7% GEC $[O_2]$, $19.34\% \pm 10.04\%$ ($p < 0.0001$); capillary RBC velocity at 2% GEC $[O_2]$, 261.2 ± 177.0 $\mu m/s$, compared to baseline 7% GEC $[O_2]$, 166.6 ± 123.7 $\mu m/s$ ($p < 0.0001$); and RBC supply rate at 2% GEC $[O_2]$, 16.80 ± 12.70 cells/s, compared to baseline 7% GEC $[O_2]$, 8.23 ± 7.40 cells/s ($p < 0.0001$) (Supplementary Figure S5).

Computer simulation results showing the steady state PO_2 within the tissue and 1000 μm micro-outlet device for high (12%) and low (2%) $[\text{O}_2]$ challenges are presented in [Supplementary Figure S6](#). Simulations of steady state conditions while the gas exchange chamber $[\text{O}_2]$ is held at 2% predicted that PO_2 within the tissue volume would be decreased by >2 mmHg up to a radial distance of 23.3 μm beyond the micro-outlet edge, and up to 67.9 μm vertically into the tissue volume in the Z-axis along the center of the circular micro-outlet ([Supplementary Figure S6](#)). Simulations for high (12%) $[\text{O}_2]$ within the gas exchange chamber predicted an increase in tissue PO_2 of >2 mmHg up to a radial distance of 59.3 μm beyond the micro-outlet edge, and a depth into the tissue volume up to 120.4 μm ([Supplementary Figure S6](#)).

4 Discussion

In this study, we developed and validated a novel thin-film micro-outlet device to deliver highly localized O_2 perturbations to regions of skeletal muscle tissue with simultaneous quantification of blood flow responses using intravital video microscopy. The knowledge obtained from previous designs, *in vivo* experiments, and the size of a single microvascular unit in rodents ($\sim 150 \times 200 \mu\text{m}$), informed our device design process ([Ghonaim et al., 2011; 2013; 2021; Sové et al., 2021; Ellis et al., 2012](#)). Laser-cut PVDC gas-impermeable film was used to pattern thin-film micro-outlets within our device to deliver oxygen perturbations into microscale tissue regions. The device was coupled with computer-controlled mass flow meters connected to a GEC for imposing $[\text{O}_2]$ perturbations to the surface of the EDL muscle overlying an inverted microscope setup. To validate the ability of our device to manipulate tissue $[\text{O}_2]$ via the GEC to the muscle, RBC SO_2 was analyzed in capillaries overlying the outlet and at various distances away from the outlet edge using IVVM and offline MATLAB software ([Ellis et al., 1990; 1992; 2012; Japee et al., 2004; Japee et al., 2005; Fraser et al., 2012; Ghonaim et al., 2021](#)).

Other groups have previously achieved the spatial specificity required to alter blood flow through induced microvascular RBC SO_2 changes *in vivo* ([Frisbee and Lombard, 2002; Frisbee et al., 2002; Ghonaim et al., 2011; 2021; Sové et al., 2021](#)). Superfusion solutions of varying O_2 levels have been used to stimulate arterioles to either vasoconstrict or vasodilate, depending on the $[\text{O}_2]$ bathing the tissue surface ([Duling and Berne, 1970a; Frisbee and Lombard, 2002; Frisbee et al., 2002; Riemann et al., 2011; Charter et al., 2018](#)). Compared to a micro-outlet device coupled to a gas exchange chamber that directly stimulates individual microvascular networks of an isolated muscle, this stimulated area in a bathed muscle preparation is much larger, affecting approximately 40-fold the microvascular surface area ([Ghonaim et al., 2011; Frisbee and Lombard, 2002; Duling and Berne, 1970a](#)). When the whole muscle is targeted in this type of preparation, multiple levels of the vasculature and associated regulatory mechanisms may be affected ([Duling and Berne, 1970a; Frisbee and Lombard, 2002; Charter et al., 2018; Russell McEvoy et al., 2022](#)). Therefore, micro-outlet devices offer more spatially constrained tissue manipulations at precise concentrations that can be changed dynamically or maintained for extended durations.

Unlike isolated muscle preparations, superfusion setups do not completely isolate the muscle from the environment ([Tym and Budreau, 1991; Riemann et al., 2011](#)). Instead, a fixed gas concentration is maintained within the solution that bathes it ([Riemann et al., 2011; Charter et al., 2018](#)). These solutions are typically equilibrated with 0% $[\text{O}_2]$ which may interfere with the interpretation of muscle blood flow, as regardless of other stimuli, the regulatory system will adjust to facilitate matching O_2 supply and demand ([Kindig et al., 2002](#)). Due to the superfusate being continuously washed away and replenished, other regulatory molecules, such as nitric oxide, may also be depleted, affecting physiological pathways and basal tone ([Jackson, 2016](#)). This may lead to confounding results in O_2 reactivity studies ([Jackson, 2016](#)). In general, oxygen has a low solubility in water, thus superfusion solutions have a finite carrying capacity which may serve as a further limiting factor. Using gas exchange chambers to stimulate the overlying muscle mitigates the consideration of O_2 solubility properties as manipulations are made in the gas phase and delivered over short diffusion distances across a gas permeable membrane ([Ellis et al., 2012; Ghonaim et al., 2011; 2021; Sové et al., 2021; Russell McEvoy et al., 2022](#)). These limitations further support the use of gas-based microfluidic approaches for studying microvascular oxygen regulation.

Through studies focused on O_2 reactivity at the microvascular level, it has been shown that when enough tissue surface is stimulated, an appropriate blood flow response will occur; a further insight on the location for O_2 sensing ([Ellis et al., 2012; Ghonaim et al., 2011; 2013; 2021; Sové et al., 2021; Russell McEvoy et al., 2022](#)). In this study, we aimed to quantify blood flow responses in individual capillary networks to gain novel insights into O_2 sensing at the capillary level. Previously, a 100 μm diameter circular outlet was shown to change RBC SO_2 in 1-2 overlying capillaries but did not stimulate a blood flow response ([Ghonaim et al., 2011](#)). RBC SO_2 manipulations in capillary networks overlying 1,000 by 200 μm micro-outlet elicited a blood flow response, suggesting that O_2 sensing and control is, at least in part, localized to capillaries ([Ghonaim et al., 2021](#)). Subsequently a similar microvascular preparation with a 400 by 200 μm micro-outlet was shown to elicit a substantial RBC SO_2 change in capillaries overlying their micro-outlets and to elicit a blood flow response by activating O_2 -mediated responses ([Sové et al., 2021](#)). Taken together, these studies demonstrate the efficacy of micro-outlet devices to manipulate the tissue microenvironment, and establish that such $[\text{O}_2]$ perturbations directed at capillaries are capable of provoking blood flow responses, yet such responses may be dependent on the number of stimulated vessels or a critical scale of tissue volume ([Ghonaim et al., 2011; 2021; Sové et al., 2021](#)).

Radial diffusion is an important characteristic of gas-based micro-outlet devices as it relates to their achievable spatial specificity. Importantly, the distance a stimulus extends into the tissue will affect how well constrained imposed $[\text{O}_2]$ perturbations are. Mathematical modelling and empirical studies have been used to describe the distribution of PO_2 in tissue overlying the micro-outlets ([Ghonaim et al., 2013](#)). The results from Ghonaim et al. suggested that imposed PO_2 changes from the GEC diffused to capillaries overlying the outlet and to capillaries up to 100 μm away. Still, logically this change in PO_2 declined over distance as the tissue returned to the mean background tissue PO_2 ([Ghonaim et al., 2013](#)).

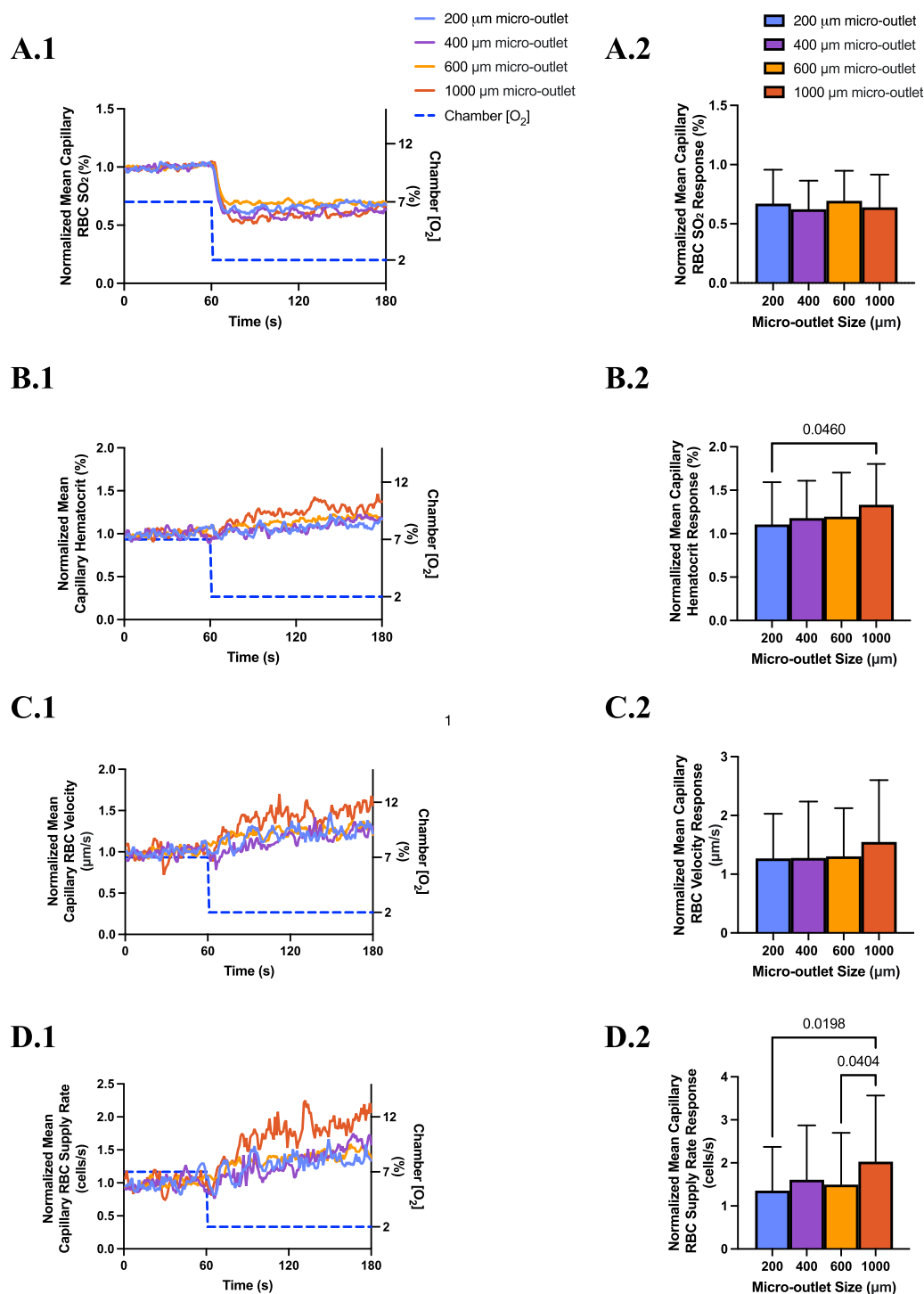


FIGURE 15

Normalized mean capillary red blood cell (RBC) oxygen saturation (SO_2) and hemodynamic responses for capillaries directly overlying the 200, 400, 600, and 1,000 μm micro-outlets in response to low (7 \rightarrow 2%) oxygen concentration ($[O_2]$) challenges. Each channel was normalized to the mean of the last 10 s of the baseline period. $[O_2]$ challenges began with 1-min baseline $[O_2]$ at 7% followed by 2 min at 2%. Time series plots are displayed in (A.1–D.1) comparing the normalized mean capillary RBC SO_2 (A.1) ($n = 43$, 200 μm ; $n = 36$, 400 μm ; $n = 79$, 600 μm ; $n = 61$, 1,000 μm), hematocrit (B.1), velocity (C.1), and supply rate (D.1), for capillaries overlying each of the four micro-outlet sizes during low $[O_2]$ challenges (for all hemodynamic channels $n = 53$, 200 μm ; $n = 36$, 400 μm ; $n = 93$, 600 μm ; $n = 73$, 1,000 μm). (A.2–D.2) represent the normalized mean responses for the last 15 s at 2% $[O_2]$ compared to the normalized baseline (7%) for capillary RBC SO_2 , hematocrit, velocity, and supply rate, in capillaries directly overlying the four micro-outlet sizes. Results show that blood flow responses are larger in magnitude for capillaries overlying larger diameter outlets versus smaller outlets. p values indicated in the figure with a $p < 0.05$ are considered significant, error bars show standard deviation of the mean.

Unfortunately, this mathematical model did not consider the gas-permeable PDMS layer directly interfaced with the muscle of interest (Ghonaïm et al., 2013; Sové et al., 2021). Therefore, O_2 perturbations in previous devices diffused more readily through the PDMS layer (due to the higher diffusivity and solubility of oxygen in PDMS), and into the muscle tissue, causing the perturbation to spread capillaries at significant distances away from the outlet (Sové et al., 2021). Therefore, this led to an underestimated radial diffusion, PO_2 distribution, and spatial specificity of the micro-outlets in the tissue (Ghonaïm et al., 2011; 2013). Further *in vivo* studies were performed, and a new model that incorporated the PDMS layer was created to aid in interpreting the results from Sové et al.'s 400 by 200 μm rectangular micro-outlet device (Sové et al., 2021). This new model and its associated *in vivo* RBC SO_2 data from capillaries at various distances away from the micro-outlets provided novel insights on the extent of O_2 spread within the PDMS layer in their device (Sové et al., 2021). The spreading effect increased this previous outlets' overall area impacted to greater than 614 by 434 μm , meaning tissue and capillaries farther than 200 μm from the outlet edge experienced significant O_2 changes (Sové et al., 2021). A comparison of low $[O_2]$ simulation results for the micro-outlet device geometry used in the present study and that used in Sové et al., 2021 is provided in **Supplementary Figure S7** for reference. Therefore, the O_2 perturbations permeate through a larger volume of tissue and vasculature than originally proposed, potentially integrating direct interactions with regulatory mechanisms in higher order vessels such as arterioles.

To determine if similar control responses would occur in a device that more precisely stimulated regions of muscle tissue, device modifications and further experiments were deemed necessary (Sové et al., 2021). With these insights in mind, our design for circular micro-outlets with diameters of 200 and 400 μm were fabricated to better determine the minimum scale of O_2 sensing and control. One of the critical device modifications that was made in the present study was changing the position of the gas permeable layer to be in contact with the GEC, and only interfaced with the muscle at the surface of the patterned micro-outlets (Ghonaïm et al., 2011; 2013; 2021; Sové et al., 2021). The purpose of this design modification was to eliminate or mitigate the effects of O_2 spreading within the PDMS that exacerbates remote changes to tissue $[O_2]$ that confounded previous studies (Sové et al., 2021).

In addition to providing greater spatial specificity, our thin-film micro-outlet devices provide superior optical properties compared to previous devices (Sové et al., 2021), which allowed us to observe and analyze capillary responses inside and outside the outlets simultaneously (Figure 2). Our micro-outlet device was designed with a thin PVDC film for the gas impermeable layer, whereas previous groups used thin glass substrates of different thicknesses ranging from 80–180 μm (Ghonaïm et al., 2011; 2013; 2021; Sové et al., 2021). When using glass substrates with air filled micro-outlets, the disparity in refractive index causes capillaries overlying the outlets to resolve at a different focal plane than those outside, even though they are at the same tissue depth (Sové et al., 2021; Figure 2). This is also a disadvantage for quantifying capillary responses overlying and outside the outlets, as the recordings must be captured separately, resulting in temporally unpaired measurements. The

PVDC film employed in our device produces a much thinner exchange membrane, provides excellent optical clarity, and as a result, the ability to analyze responses of capillaries overlying and outside the outlets simultaneously during $[O_2]$ oscillations and challenges.

4.1 Oxygen oscillations

In our study, we altered muscle $[O_2]$ concentrations using a gas-based micro-outlet device and GEC that was directly interfaced with the EDL muscle. As expected, the 4-min $[O_2]$ oscillations in the GEC were able to induce rapid and profound alterations in capillary RBC SO_2 in capillaries overlying the 400 μm micro-outlets without affecting the SO_2 in capillaries outside the outlets. The SO_2 measurements validated our device's ability to impose rapid localized gas-based perturbations without altering the tissue microenvironment in neighboring vessels outside the micro-outlet. Capillary RBC SO_2 changes in the tissue occurred rapidly, reaching their mean peak responses within 12 s at 12% $[O_2]$ (86.9%) and 11 s at 2% $[O_2]$ (43.5%) (Figure 3).

Significant hemodynamic responses in capillaries directly overlying the 400 μm micro-outlets occurred without affecting neighboring vessels adjacent to the micro-outlet during $[O_2]$ oscillations (Figures 3, 4). Specifically, significant differences were observed for RBC supply rate, velocity, and hematocrit levels between 12% and 2% $[O_2]$ oscillations (Figure 3). Interestingly, there was a significant difference in mean RBC supply rate between the first, baseline 7% $[O_2]$ and the last 7%, where we expected to see similar flow states as both time periods were collected at the same baseline $[O_2]$. This data suggests that 1 min at baseline 7% may not be enough time for the flow to normalize after it undergoes high and low 1-min $[O_2]$ oscillations; this is interpreted further below.

During $[O_2]$ oscillations, hematocrit levels were only significantly different between 12% and 2% GEC $[O_2]$ (Figure 3), suggesting hematocrit levels do not modulate readily to $[O_2]$ perturbations slightly above or below baseline conditions. It was presented in the literature by Kindig et al. and supported by Russell McEvoy et al. that transient changes in hematocrit are a result of diameter changes in higher order arterioles altering hematocrit levels of downstream vessels based on the Fåhræus effect (Fåhræus and Lindqvist, 1931; Barbee and Cokelet, 1971; Pries et al., 1986; Kindig et al., 2002; Russell McEvoy et al., 2022). Since the microvascular region affected is highly confined in our 200 and 400 μm micro-outlets, it is unlikely that higher order arterioles are stimulated; thus, vasoactive responses in terminal arterioles would not result in significant changes in hematocrit during $[O_2]$ oscillations. Therefore, the number of capillaries stimulated by O_2 perturbations was enough to elicit a flow increase in response to low $[O_2]$ conditions but not a consistent decrease at high $[O_2]$ conditions.

There were significant increases in velocity and supply rate between the initial 1 min 7% $[O_2]$ and the second 7% $[O_2]$ condition, which suggests flow did not return to baseline after increasing during the 2% $[O_2]$. A study published by our group using full tissue surface perturbations described time transients during 2→7% $[O_2]$ challenges with their associated mean peak responses in capillary RBC velocity ($t = 77$ s), hematocrit, ($t = 105$ s), and supply

rate ($t = 76$ s) (Russell McEvoy et al., 2022). Such results suggest that after a 1-min oscillation at 2%, the baseline hemodynamic responses to 7% $[O_2]$ did not have enough time to provoke a full response in the 1-min oscillation. Therefore, this may explain why we found a significant increase between our first and last baseline 7% minute.

Capillaries analyzed in our 400 μm diameter micro-outlets did not experience a significant decrease in hemodynamic values between baseline 7% and 12% $[O_2]$ during oscillations. There are a few potential reasons for this result. Compared to previous studies, our results suggest the chosen outlet sizes could not perturb the vasculature sufficiently to initiate O_2 sensing mechanisms to react when $[O_2]$ was increased to 12% (Ghonaim et al., 2011; 2021; Sové et al., 2021; Russell McEvoy et al., 2022). Russell McEvoy et al., provided evidence to show that 7 \rightarrow 12% and 7 \rightarrow 2% $[O_2]$ changes provoke regulatory responses that are asymmetric and that when $[O_2]$ is increased from baseline, the hemodynamic regulatory response is not as profound as it is when $[O_2]$ is decreased to 2%. This is possibly due to a more robust change in capillary RBC SO_2 between 7 \rightarrow 2% GEC $[O_2]$ which provoked a 29.5% decrease in RBC SO_2 compared to a 19.7% increase in RBC SO_2 for the 7 \rightarrow 12% GEC $[O_2]$ (Russell McEvoy et al., 2022). Thus, the more profound the RBC SO_2 change, the greater the elicited flow response. Our oscillation data supports this conclusion as we observed significant hemodynamic increases during low 2% $[O_2]$ oscillations compared to baseline 7%. Furthermore, in some previous micro-outlet studies, the baseline GEC $[O_2]$ used was 5% (Ghonaim et al., 2011; 2021; Sové et al., 2021), and high $[O_2]$ was 12% or 20%, creating a considerably more forceful step change in $[O_2]$ compared to the present study (Ghonaim et al., 2011; 2021; Sové et al., 2021). Significant hemodynamic differences were found during similar high $[O_2]$ conditions in previous studies, but their oscillations were longer than in our current work, with high and low step changes occurring for 2 min each (Sové et al., 2021; Ghonaim et al., 2021). Therefore, inducing sequential high and low $[O_2]$ perturbations may interfere with the ability of the control system to reach a peak hemodynamic response over the observation period. It is also plausible that the signaling pathways linking RBC SO_2 with functional hemodynamic responses are non-linear, which could be a result of enhanced ATP release at lower SO_2 , luminal ATP concentration dependence to trigger endothelial cell hyperpolarization, or other as yet undefined oxygen-dependent mechanisms within the transduction pathway. Lastly, the location of terminal arterioles supplying the network of interest and their distance from an outlet may influence the ability to modulate blood flow. Studies that stimulated larger areas of muscle tissue are more likely to interact with terminal arterioles, or higher vasculature (Ghonaim et al., 2021; Sové et al., 2021; Russell McEvoy et al., 2022). Modulating tissue $[O_2]$ both at a terminal arteriole and its downstream capillary network may result in a more robust or rapid regulatory response.

4.2 Oxygen challenges

As expected, high (7 \rightarrow 12%) and low (7 \rightarrow 2%) $[O_2]$ challenges from the gas exchange chamber caused rapid and profound

alterations in capillary RBC SO_2 in capillaries overlying the 400 μm micro-outlets without causing significant changes in capillary RBC SO_2 outside the outlets (Figures 5–8). Additionally, capillaries less than 100 μm away from the 200 μm outlets experienced significant but comparatively small RBC SO_2 changes during high $[O_2]$ challenges (Figure 11). Compared to the RBC SO_2 change experienced by capillaries directly overlying the micro-outlet, capillaries less than 100 μm away from the outlet edge changed from 42.2% to 47.2%, whereas the capillaries overlying the micro-outlet experienced an increase from 60.7% to 80.0% RBC SO_2 (Figures 10, 11). Our data shows that the area of effect for our 200 μm diameter micro-outlets is within 100 μm of the micro-outlet edge when imposing 2-min $[O_2]$ challenges. Interestingly, for the 2% $[O_2]$ condition, our model predicted changes in tissue PO_2 of >2 mmHg up to a radial distance of 17 μm from the 400 μm micro-outlet, though we did not find any significant changes in capillary RBC SO_2 in the <100 μm distance range. This is likely due to the small number of capillaries available to be analyzed in the region within 17 μm of the outlet edge, with a larger proportion of measurements in the <100 μm distance bin coming from vessels 17–100 μm from the micro-outlet. Furthermore, since the perturbation in tissue PO_2 drops exponentially with distance from the micro-outlet, capillaries at a distance are more resistant to changes in SO_2 as they are supplied with ‘fresh’ RBCs from tissue volumes that are unperturbed by the micro-outlet $[O_2]$.

The 7 \rightarrow 2% $[O_2]$ challenges induced significant hemodynamic responses in capillaries directly overlying 400 μm micro-outlets, as determined by increased mean RBC supply rate and velocity (Figure 7). Significant hemodynamic decreases were observed during high $[O_2]$ challenges in capillaries overlying the 400 μm diameter outlets (Figure 5). This is an exciting finding as we did not observe significant responses between 7% and 12% during our 4-min oscillations. This finding supports our interpretation of a time-dependent effect related to stimulating O_2 regulatory mechanisms in high $[O_2]$ areas in small muscle tissue regions. Significant hematocrit changes occurred during low $[O_2]$ challenges but not during high $[O_2]$ challenges.

Although some flow responses did occur in vessels outside the 200 μm outlets, there were no corresponding mean RBC SO_2 changes in these vessels. The changes in flow outside the 200 μm diameter micro-outlets may be a result of conducted signaling from vasculature overlying the micro-outlets, directly connected with vessels at a distance (Collins et al., 1998; McCullough et al., 1997; Bagher and Segal, 2011). If stimulating a capillary network overlying the micro-outlet affected capillary networks connected to the same feed arteriole situated outside the outlet, it would support the role of conducted signaling in the response (Collins et al., 1998; Ellsworth, 2004; Ellsworth et al., 2009; Ellis et al., 2012; Ghonaim et al., 2011). In comparison, Sové et al., did not obtain robust hemodynamic changes in capillaries at a distance from their outlets, though details regarding this data were not reported. Still, they provide data showing profound changes in RBC SO_2 in capillaries measured at three distances reaching farther than 200 μm from the outlet edge. Based on the significant SO_2 changes found, it is surprising that they did not observe corresponding flow changes in these capillaries as they did in capillaries overlying outlets. However, based on our knowledge of the study, this was due to a relatively small number

of remote capillaries available to be sampled for comparisons (Sové et al., 2021).

Hemodynamic responses were observed in capillaries outside the 400 μm diameter outlets at distances farther than 100 μm away but not in vessels less than 100 μm away during low $[\text{O}_2]$ challenges. This observation showed a 25% supply rate increase in capillaries 200 μm away from the outlet compared to a 65% mean supply rate increase in vessels directly crossing the outlets (Figures 7, 8). These hemodynamic changes remote to the micro-outlets may be due to conducted signaling between interconnected vasculature, as mentioned above. In our devices and in previous devices, multiple micro-outlets are in contact with the muscle within a relatively small region of the tissue surface (Sové et al., 2021). In our devices, adjacent micro-outlets are separated by 1,000 μm . Since the microcirculation is highly interconnected, vessels overlying the micro-outlets that experience a supply rate change may also induce a supply rate change in vessels at a distance from the outlet; one that may be unrelated to the local tissue micro-environment in these remote vessels. Multiple micro-outlets may stimulate responses remote to the confined stimulated region, which is more likely to cause significant supply rate changes in outside vessels.

It has been proposed repeatedly in the literature that capillaries are involved in oxygen-mediated blood flow regulation (Ellsworth et al., 1995; Ellsworth et al., 2009; Ellis et al., 2012; Dietrich and Tyml, 1992; Song and Tyml, 1993; Ghonaim et al., 2011; Ghonaim et al., 2013; Ghonaim et al., 2021; Sové et al., 2021; Lamb et al., 2021). Capillaries are suggested to play a role in sensing local O_2 conditions via SO_2 -dependent ATP release from erythrocytes which then initiates conducted signaling to arterioles upstream (Collins et al., 1998; Dietrich et al., 2009; Arciero et al., 2008; Ellsworth et al., 2009; Dora, 2017). Our observations further demonstrate that the magnitude of capillary RBC supply rate responses are closely coupled with capillary RBC SO_2 . In the case of our micro-outlet devices, the fixed PO_2 condition at the exchange surface effectively clamps capillary RBC SO_2 , which, in conjunction with the resulting supply rate response, imposes a static stimulus to the regulatory system that is analogous to a highly localized change in tissue O_2 consumption. *In situ*, increases in whole muscle O_2 consumption during exercise are similarly accommodated by proportional increases in blood flow and O_2 extraction, thus matching total tissue O_2 demand with supply (Andersen and Saltin, 1985; Casaburi et al., 1989). The present study provides direct evidence that O_2 demand-supply matching occurs at or below the scale of single capillary units, and implies that fine regulatory control of blood flow distribution within tissues is necessary to satisfy changes in overall O_2 demand.

It has also been hypothesized that the magnitude of the flow responses observed in relation to $[\text{O}_2]$ perturbations is proportional to the number of capillaries and endothelial cells stimulated within a network (Ellis et al., 2012; Ghonaim et al., 2013; 2021; Sové et al., 2021). Our results for different outlet sizes support this hypothesis, as in 7–2% $[\text{O}_2]$ challenges we observed a 38% increase in capillary RBC supply rate in the 200 μm diameter outlets, a 65% increase in 400 μm outlets, and a 104% increase in 1,000 μm , despite similar changes in capillary RBC SO_2 (Figure 15). Indeed, the normalized comparison of low O_2

challenge responses for the four sizes of micro-outlets suggests that larger micro-outlets provoke a greater and more vigorous responses (Figure 15). During high $[\text{O}_2]$ challenges, our 200 μm diameter micro-outlets did not provoke a significant decrease in capillary RBC supply rate, but mean capillary RBC supply rate did have a significant decrease of 12% in the 400 μm micro-outlets. Endothelial cells in skeletal muscle are approximately 104 μm long, and microvascular units are typically $150 \times 200 \mu\text{m}$ in rodents (Adamson, 1993; Yuan and Rigor, 2010), so a larger outlet would be expected to stimulate more endothelial cells to hyperpolarize and contribute to a conducted response from $[\text{O}_2]$ changes. Therefore, the larger the micro-outlet device and muscle tissue area stimulated by $[\text{O}_2]$ perturbations, the greater the potential flow response. This is likely due to the integration of conducted signals reaching arterioles reflecting hyperpolarization of the capillary endothelium from multiple capillaries that the arteriole supplies (McCullough et al., 1997; Collins et al., 1998; Lidington et al., 2002; Dietrich et al., 2009; Ellis et al., 2012; Dora, 2016). Therefore, the magnitude of the flow response should be at least in part reflected by the number of endothelial cells and individual capillaries influenced by the micro-outlet perturbation (Ghonaim et al., 2011; 2013), and not just the change in capillary RBC SO_2 . Furthermore, in 100 μm outlet affecting 1–2 capillaries via $[\text{O}_2]$ perturbations did not elicit a flow response (Ghonaim et al., 2011), but our 200 μm micro-outlet affecting approximately double the capillaries and endothelial cells, did yield significant hemodynamic responses. Therefore, our results support the concept of spatially summative responses and provide evidence for capillary level O_2 sensing.

Our significant capillary hemodynamic responses from 200 μm diameter micro-outlets represent a promising means to manipulate blood flow via $[\text{O}_2]$ at the capillary level without directly stimulating higher levels of the vasculature. As discussed above, flow responses observed in our small, circular 200 μm diameter micro-outlets indicate that individual capillary networks can sense O_2 and precisely modulate local blood flow in response. In previous studies, micro-outlet devices could not achieve a blood flow response to a stimulus of this small size, therefore, our findings provide novel insights into the scale of O_2 sensing. Future studies should aim to quantify the O_2 flux from capillaries overlying the micro-outlet device to more directly describe how changes in O_2 extraction in the stimulated capillaries relate to the modulation of supply rate, and hence O_2 supply at this scale.

In conclusion, we have developed and validated a thin-film micro-outlet device that can elicit $[\text{O}_2]$ perturbations within highly confined regions of skeletal muscle tissue, effectively modulating local capillary RBC SO_2 and provoking corresponding flow responses in micro-outlets as small as 200 μm in diameter. Our novel micro-outlet devices have also demonstrated superior optical properties that allow for temporally matched comparisons between capillaries directly overlying the micro-outlet and vessels at a distance from the stimulus.

In future studies, our device can be used to obtain the high level of spatial specificity necessary to interrogate capillary level regulation mechanisms using multi-modal approaches, such as intravascular pharmacological interventions. Our modular device can easily be modified to address a wide range of research

questions and is suitable for future studies to target various levels of microcirculation and specific mechanisms responsible for oxygen-mediated blood flow regulation.

Data availability statement

The raw data supporting the conclusions of this article will be made available by the authors, without undue reservation.

Ethics statement

The animal study was approved by Memorial University Animal Care Committee. The study was conducted in accordance with the local legislation and institutional requirements.

Author contributions

MK: Conceptualization, Data curation, Formal Analysis, Investigation, Methodology, Visualization, Writing – original draft, Writing – review and editing. RJS: Conceptualization, Formal Analysis, Methodology, Software, Visualization, Writing – original draft, Writing – review and editing. RHS: Investigation, Writing – review and editing. BW: Investigation, Writing – review and editing. GRM: Data curation, Formal Analysis, Investigation, Writing – review and editing. GF: Conceptualization, Formal Analysis, Funding acquisition, Investigation, Methodology, Project administration, Resources, Software, Supervision, Visualization, Writing – original draft, Writing – review and editing.

Funding

The author(s) declare that financial support was received for the research and/or publication of this article. This work was supported by the Natural Sciences and Engineering Research Council of Canada Discovery grant RGPIN 2017-05205 to GMF. NSERC funding supplied resources for experimental materials, equipment, technical support, and trainee stipends.

References

- Adamson, R. H. (1993). Microvascular endothelial cell shape and size *in situ*. *Microvasc. Res.* 46 (1), 77–88. doi:10.1006/mvres.1993.1036
- Andersen, P., and Saltin, B. (1985). Maximal perfusion of skeletal muscle in man. *J. Physiol.* 366, 233–249. doi:10.1113/jphysiol.1985.sp015794
- Arciero, J. C., Carlson, B. E., and Secomb, T. W. (2008). Theoretical model of metabolic blood flow regulation: roles of ATP release by red blood cells and conducted responses. *Am. J. physiology. Heart circulatory physiology* 295 (4), H1562–H1571. doi:10.1152/ajpheart.00261.2008
- Bagher, P., and Segal, S. S. (2011). Regulation of blood flow in the microcirculation: role of conducted vasodilation. *Acta physiol. Oxf. Engl.* 202 (3), 271–284. doi:10.1111/j.1748-1716.2010.02244.x
- Barbee, J. H., and Cokelet, G. R. (1971). The Fahraeus effect. *Microvasc. Res.* 3 (1), 6–16. doi:10.1016/0026-2862(71)90002-1
- Bergfeld, G., and Forrester, T. (1992). Release of ATP from human erythrocytes in response to a brief period of hypoxia and hypercapnia. *Cardiovasc. Res.* 26 (1), 40–47. doi:10.1093/cvr/26.1.40
- Buehler, P. W., and Alayash, A. I. (2004). Oxygen sensing in the circulation: “cross talk” between red blood cells and the vasculature. *Antioxidants and redox Signal.* 6 (6), 1000–1010. doi:10.1089/ars.2004.6.1000
- Busse, R., Förstermann, U., Matsuda, H., and Pohl, U. (1984). The role of prostaglandins in the endothelium-mediated vasodilatory response to hypoxia. *Pflügers Archiv Eur. J. physiology* 401 (1), 77–83. doi:10.1007/BF00581536
- Busse, R., Pohl, U., Kellner, C., and Klemm, U. (1983). Endothelial cells are involved in the vasodilatory response to hypoxia. *Pflügers Archiv Eur. J. physiology* 397 (1), 78–80. doi:10.1007/BF00581575
- Carlson, B. E., and Secomb, T. W. (2005). A theoretical model for the myogenic response based on the length-tension characteristics of vascular

Acknowledgments

We would like to thank NSERC for funding this project. Special thanks to MUN MED 3D printing services for the printing of our gas exchange chamber microscope components. We thank Chris Ellis and Stephanie Milkovich from Western University for providing sample images from a previous study (Sové et al., 2021) to include in Figure 2. Also, we could not have fabricated our devices without the high precision laser cutting work of mechanical technologists Matthew Fudge and Evan Kearley from Engineering Technical Services of Memorial University.

Conflict of interest

The authors declare that the research was conducted in the absence of any commercial or financial relationships that could be construed as a potential conflict of interest.

Generative AI statement

The author(s) declare that no Generative AI was used in the creation of this manuscript.

Publisher's note

All claims expressed in this article are solely those of the authors and do not necessarily represent those of their affiliated organizations, or those of the publisher, the editors and the reviewers. Any product that may be evaluated in this article, or claim that may be made by its manufacturer, is not guaranteed or endorsed by the publisher.

Supplementary material

The Supplementary Material for this article can be found online at: <https://www.frontiersin.org/articles/10.3389/fphys.2025.1575776/full#supplementary-material>

- smooth muscle. *Microcirc. (New York, N.Y. 1994)* 12 (4), 327–338. doi:10.1080/10739680590934745
- Casaburi, R., Daly, J., Hansen, J. E., and Effros, R. M. (1989). Abrupt changes in mixed venous blood gas composition after the onset of exercise. *J. Appl. Physiol.* 67 (3), 1106–1112. doi:10.1152/jappl.1989.67.3.1106
- Charter, M. E., Lamb, I. R., and Murrant, C. L. (2018). Arteriolar and capillary responses to CO₂ and H⁺ in hamster skeletal muscle microvasculature: implications for active hyperemia. *Microcirc. (New York, N.Y. 1994)* 25 (7), e12494. doi:10.1111/micc.12494
- Coburn, R. F., Grubb, B., and Aronson, R. D. (1979). Effect of cyanide on oxygen tension-dependent mechanical tension in rabbit aorta. *Circulation Res.* 44 (3), 368–378. doi:10.1161/01.res.44.3.368
- Collins, D. M., McCullough, W. T., and Ellsworth, M. L. (1998). Conducted vascular responses: communication across the capillary bed. *Microvasc. Res.* 56, 43–53. doi:10.1006/mvres.1998.2076
- Delp, M. D. (1999). Control of skeletal muscle perfusion at the onset of dynamic exercise. *Med. Sci. Sports Exerc.* 31 (7), 1011–1018. doi:10.1097/00005768-199907000-00014
- Dietrich, H. H. (1989). Effect of locally applied epinephrine and norepinephrine on blood flow and diameter in capillaries of rat mesentery. *Microvasc. Res.* 38 (2), 125–135. doi:10.1016/0026-2862(89)90021-6
- Dietrich, H. H., Ellsworth, M. L., Sprague, R. S., and Dacey, R. G., Jr (2000). Red blood cell regulation of microvascular tone through adenosine triphosphate. *Am. J. physiology. Heart circulatory physiology* 278 (4), H1294–H1298. doi:10.1152/ajpheart.2000.278.4.H1294
- Dietrich, H. H., Horiuchi, T., Xiang, C., Hongo, K., Falck, J. R., and Dacey, R. G., Jr (2009). Mechanism of ATP-induced local and conducted vasomotor responses in isolated rat cerebral penetrating arterioles. *J. Vasc. Res.* 46 (3), 253–264. doi:10.1159/000167273
- Dietrich, H. H., and Tyml, K. (1992). Capillary as a communicating medium in the microvasculature. *Microvasc. Res.* 43 (1), 87–99. doi:10.1016/0026-2862(92)90008-d
- Dora, K. A. (2016). Endothelial-smooth muscle cell interactions in the regulation of vascular tone in skeletal muscle. *Microcirc. (New York, N.Y. 1994)* 23 (8), 626–630. doi:10.1111/micc.12322
- Dora, K. A. (2017). Conducted dilatation to ATP and K⁺ in rat skeletal muscle arterioles. *Acta physiol. Oxf. Engl.* 219 (1), 202–218. doi:10.1111/apha.12656
- Duling, B. R. (1972). Microvascular responses to alterations in oxygen tension. *Circulation Res.* 31 (4), 481–489. doi:10.1161/01.res.31.4.481
- Duling, B. R. (1973). The preparation and use of the hamster cheek pouch for studies of the microcirculation. *Microvasc. Res.* 5 (3), 423–429. doi:10.1016/0026-2862(73)90059-9
- Duling, B. R. (1974). Oxygen sensitivity of vascular smooth muscle. II. *in vivo* studies. *Am. J. physiology* 227 (1), 42–49. doi:10.1152/ajplegacy.1974.227.1.42
- Duling, B. R., and Berne, R. M. (1970a). Longitudinal gradients in periarteriolar oxygen tension. A possible mechanism for the participation of oxygen in local regulation of blood flow. *Circulation Res.* 27 (5), 669–678. doi:10.1161/01.res.27.5.669
- Duling, B. R., and Berne, R. M. (1970b). Propagated vasodilation in the microcirculation of the hamster cheek pouch. *Circulation Res.* 26 (2), 163–170. doi:10.1161/01.res.26.2.163
- Duling, B. R., and Klitzman, B. (1980). Local control of microvascular function: role in tissue oxygen supply. *Annu. Rev. physiology* 42, 373–382. doi:10.1146/annurev.ph.42.030180.002105
- Ellis, C. G., Ellsworth, M. L., and Pittman, R. N. (1990). Determination of red blood cell oxygenation *in vivo* by dual video densitometric image analysis. *Am. J. physiology* 258 (4 Pt 2), H1216–H1223. doi:10.1152/ajpheart.1990.258.4.H1216
- Ellis, C. G., Ellsworth, M. L., Pittman, R. N., and Burgess, W. L. (1992). Application of image analysis for evaluation of red blood cell dynamics in capillaries. *Microvasc. Res.* 44 (2), 214–225. doi:10.1016/0026-2862(92)90081-y
- Ellis, C. G., Jagger, J., and Sharpe, M. (2005). The microcirculation as a functional system. *Crit. care London, Engl.* 9 (Suppl. 4), S3–S8. doi:10.1186/cc3751
- Ellis, C. G., Milkovich, S., and Goldman, D. (2012). What is the efficiency of ATP signaling from erythrocytes to regulate distribution of O₂ supply within the microvasculature? *Microcirc. (New York, N.Y. 1994)* 19 (5), 440–450. doi:10.1111/j.1549-8719.2012.00196.x
- Ellsworth, M. L. (2004). Red blood cell-derived ATP as a regulator of skeletal muscle perfusion. *Med. Sci. Sports Exerc.* 36 (1), 35–41. doi:10.1249/01.MSS.0000106284.80300.B2
- Ellsworth, M. L., Ellis, C. G., Goldman, D., Stephenson, A. H., Dietrich, H. H., and Sprague, R. S. (2009). Erythrocytes: oxygen sensors and modulators of vascular tone. *Physiol. Bethesda, Md.* 24, 107–116. doi:10.1152/physiol.00038.2008
- Ellsworth, M. L., Forrester, T., Ellis, C. G., and Dietrich, H. H. (1995). The erythrocyte as a regulator of vascular tone. *Am. J. physiology* 269 (6 Pt 2), H2155–H2161. doi:10.1152/ajpheart.1995.269.6.H2155
- Fåhræus, R., and Lindqvist, R. (1931). The viscosity of the blood in narrow capillary tubes. *Am. J. Physiol.* 96, 562–568. doi:10.1152/ajplegacy.1931.96.3.562
- Fraser, G. M., Milkovich, S., Goldman, D., and Ellis, C. G. (2012). Mapping 3-D functional capillary geometry in rat skeletal muscle *in vivo*. *Am. J. Physiol. Heart Circ. Physiol.* 302 (3), H654–H664. doi:10.1152/ajpheart.01185.2010
- Fredricks, K. T., Liu, Y., and Lombard, J. H. (1994). Response of extraparenchymal resistance arteries of rat skeletal muscle to reduced PO₂. *Am. J. Physiol.* 267 (2 Pt 2), H706–H715. doi:10.1152/ajpheart.1994.267.2.H706
- Frisbee, J. C. (2001). Impaired dilation of skeletal muscle microvessels to reduced oxygen tension in diabetic obese Zucker rats. *Am. J. physiology. Heart circulatory physiology* 281 (4), H1568–H1574. doi:10.1152/ajpheart.2001.281.4.H1568
- Frisbee, J. C., and Lombard, J. H. (2002). Parenchymal tissue cytochrome P450 4A enzymes contribute to oxygen-induced alterations in skeletal muscle arteriolar tone. *Microvasc. Res.* 63 (3), 340–343. doi:10.1006/mvres.2002.2409
- Frisbee, J. C., Maier, K. G., Falck, J. R., Roman, R. J., and Lombard, J. H. (2002). Integration of hypoxic dilation signaling pathways for skeletal muscle resistance arteries. *Am. J. Physiol. Regul. Integr. Compar. Physiol.* 283, R309–R319. doi:10.1152/ajpregu.00741.2001
- Frisbee, J. C., Roman, R. J., Krishna, U. M., Falck, J. R., and Lombard, J. H. (2001). Relative contributions of cyclooxygenase- and cytochrome P450 omega-hydroxylase-dependent pathways to hypoxic dilation of skeletal muscle resistance arteries. *J. Vasc. Res.* 38 (4), 305–314. doi:10.1159/000051061
- Frisbee, J. C., and Stepp, D. W. (2001). Impaired NO-dependent dilation of skeletal muscle arterioles in hypertensive diabetic obese Zucker rats. *Am. J. physiology. Heart circulatory physiology* 281 (3), H1304–H1311. doi:10.1152/ajpheart.2001.281.3.H1304
- Ghonaim, N. W., Fraser, G. M., Ellis, C. G., Yang, J., and Goldman, D. (2013). Modeling steady state SO₂-dependent changes in capillary ATP concentration using novel O₂ micro-delivery methods. *Front. physiology* 4, 260. doi:10.3389/fphys.2013.00260
- Ghonaim, N. W., Fraser, G. M., Goldman, D., Milkovich, S., Yang, J., and Ellis, C. G. (2021). Evidence for role of capillaries in regulation of skeletal muscle oxygen supply. *Microcirc. (New York, N.Y.:1994)* 28 (6), e12699. doi:10.1111/micc.12699
- Ghonaim, N. W., Lau, L. W., Goldman, D., Ellis, C. G., and Yang, J. (2011). A micro-delivery approach for studying microvascular responses to localized oxygen delivery. *Microcirc. (New York, N.Y.:1994)* 18 (8), 646–654. doi:10.1111/j.1549-8719.2011.00132.x
- Golub, A. S., and Pittman, R. N. (2013). Bang-bang model for regulation of local blood flow. *Microcirc. (New York, N.Y. 1994)* 20 (6), 455–483. doi:10.1111/micc.12051
- González-Alonso, J. (2012). ATP as a mediator of erythrocyte-dependent regulation of skeletal muscle blood flow and oxygen delivery in humans. *J. Physiol.* 590 (20), 5001–5013. doi:10.1113/jphysiol.2012.235002
- Harder, D. R., Narayanan, J., Birks, E. K., Liard, J. F., Imig, J. D., Lombard, J. H., et al. (1996). Identification of a putative microvascular oxygen sensor. *Circulation Res.* 79 (1), 54–61. doi:10.1161/01.res.79.1.54
- Hester, R. L. (1993). Uptake of metabolites by postcapillary venules: mechanism for the control of arteriolar diameter. *Microvasc. Res.* 46 (2), 254–261. doi:10.1006/mvres.1993.1050
- Hutchins, P. M., Bond, R. F., and Green, H. D. (1974). Participation of oxygen in the local control of skeletal muscle microvasculature. *Circulation Res.* 34 (1), 85–93. doi:10.1161/01.res.40.4.85
- Jackson, W. F. (1986). Prostaglandins do not mediate arteriolar oxygen reactivity. *Am. J. physiology* 250 (6 Pt 2), H1102–H1108. doi:10.1152/ajpheart.1986.250.6.H1102
- Jackson, W. F. (2016). Arteriolar oxygen reactivity: where is the sensor and what is the mechanism of action? *J. Physiol.* 594 (18), 5055–5077. doi:10.1113/jp270192
- Jackson, W. F., and Duling, B. R. (1983). The oxygen sensitivity of hamster cheek pouch arterioles. *in vitro and in situ studies. Circulation Res.* 53 (4), 515–525. doi:10.1161/01.res.53.4.515
- Jackson, W. F., Pohl, U., and Busse, R. (1987). Endothelium-dependent oxygen reactivity in hamster carotid arteries. *Fed. Proc.* 46, 1530.
- Jagger, J. E., Bateman, R. M., Ellsworth, M. L., and Ellis, C. G. (2001). Role of erythrocyte in regulating local O₂ delivery mediated by hemoglobin oxygenation. *Am. J. physiology. Heart circulatory physiology* 280 (6), H2833–H2839. doi:10.1152/ajpheart.2001.280.6.H2833
- Japee, S. A., Ellis, C. G., and Pittman, R. N. (2004). Flow visualization tools for image analysis of capillary networks. *Microcirc. (New York, N.Y. 1994)* 11 (1), 39–54. doi:10.1080/10739680490266171
- Japee, S. A., Pittman, R. N., and Ellis, C. G. (2005). A new video image analysis system to study red blood cell dynamics and oxygenation in capillary networks. *Microcirc. (New York, N.Y. 1994)* 12 (6), 489–506. doi:10.1080/10739680591003332
- Jia, L., Bonaventura, C., Bonaventura, J., and Stamler, J. S. (1996). S-nitrosohaemoglobin: a dynamic activity of blood involved in vascular control. *Nature* 380, 221–226. doi:10.1038/380221a0

- Kerkhof, C. J., Bakker, E. N., and Sipkema, P. (1999). Role of cytochrome P-450 4A in oxygen sensing and NO production in rat cremaster resistance arteries. *Am. J. physiology* 277 (4), H1546–H1552. doi:10.1152/ajpheart.1999.277.4.H1546
- Kindig, C. A., Richardson, T. E., and Poole, D. C. (2002). Skeletal muscle capillary hemodynamics from rest to contractions: implications for oxygen transfer. *J. Appl. physiology (Bethesda, Md. 1985)* 92 (6), 2513–2520. doi:10.1152/japplphysiol.01222.2001
- Kowalewska, P. M., Milkovich, S. L., Goldman, D., Sandow, S. L., Ellis, C. G., and Welsh, D. G. (2024). Capillary oxygen regulates demand-supply coupling by triggering connexin40-mediated conduction: rethinking the metabolic hypothesis. *Proc. Natl. Acad. Sci. U. S. A.* 121 (8), e2303119121. doi:10.1073/pnas.2303119121
- Lamb, I. R., Novielli-Kuntz, N. M., and Murrant, C. L. (2021). Capillaries communicate with the arteriolar microvascular network by a pannexin/purinergic-dependent pathway in hamster skeletal muscle. *Am. J. physiology: Heart circulatory physiology* 320 (4), H1699–H1711. doi:10.1152/ajpheart.00493.2020
- Laughlin, M. H., Davis, M. J., Secher, N. H., van Lieshout, J. J., Arce-Esquivel, A. A., Simmons, G. H., et al. (2012). Peripheral circulation. *Compr. Physiol.* 2 (1), 321–447. doi:10.1002/cphy.c100048
- Lidington, D., Ouellette, Y., and Tymk, K. (2002). Communication of agonist-induced electrical responses along 'capillaries' *in vitro* can be modulated by lipopolysaccharide, but not nitric oxide. *J. Vasc. Res.* 39 (5), 405–413. doi:10.1159/000064519
- McCullough, W. T., Collins, D. M., and Ellsworth, M. L. (1997). Arteriolar responses to extracellular ATP in striated muscle. *Am. J. Physiol.* 272, H1886–H1891. doi:10.1152/ajpheart.1997.272.4.h1886
- Messina, L. M., Ekhterae, D., Whitehill, T. A., Podrazik, R. M., Burkell, W. E., Ford, J., et al. (1994). Transplantation of lac-Z-transduced microvascular endothelial cells into the skeletal muscle capillary bed of the rat hindlimb occurs independent of the duration of femoral artery occlusion after injection of cells. *J. Surg. Res.* 57 (6), 661–666. doi:10.1006/jsre.1994.1197
- Messina, L. M., Podrazik, R. M., Whitehill, T. A., Ekhterae, D., Brothers, T. E., Wilson, J. M., et al. (1992). Adhesion and incorporation of lacZ-transduced endothelial cells into the intact capillary wall in the rat. *Proc. Natl. Acad. Sci. U. S. A.* 89 (24), 12018–12022. doi:10.1073/pnas.89.24.12018
- Ngo, A. T., Jensen, L. J., Riemann, M., Holstein-Rathlou, N. H., and Torp-Pedersen, C. (2010). Oxygen sensing and conducted vasomotor responses in mouse cremaster arterioles *in situ*. *Pflügers Archiv Eur. J. physiology* 460 (1), 41–53. doi:10.1007/s00424-010-0837-x
- Olsson, R. A. (1981). Local factors regulating cardiac and skeletal muscle blood flow. *Annu. Rev. physiology* 43, 385–395. doi:10.1146/annurev.ph.43.030181.002125
- Patel, S., Joseph, S. K., and Thomas, A. P. (1999). Molecular properties of inositol 1,4,5-trisphosphate receptors. *Cell calcium* 25 (3), 247–264. doi:10.1054/ceca.1999.0021
- Pittman, R. N., and Duling, B. R. (1973). Oxygen sensitivity of vascular smooth muscle. I. *in vitro* studies. *Microvasc. Res.* 6 (2), 202–211. doi:10.1016/0026-2862(73)90020-4
- Pohl, U., and Busse, R. (1989). Hypoxia stimulates release of endothelium-derived relaxant factor. *Am. J. physiology* 256 (6 Pt 2), H1595–H1600. doi:10.1152/ajpheart.1989.256.6.H1595
- Pohl, U., De Wit, C., and Gloe, T. (2000). Large arterioles in the control of blood flow: role of endothelium-dependent dilation. *Acta physiol. Scand.* 168 (4), 505–510. doi:10.1046/j.1365-201x.2000.00702.x
- Potter, R. F., Dietrich, H. H., Tymk, K., Ellis, C. G., Cronkwright, J., and Groom, A. C. (1993). Ischemia-reperfusion induced microvascular dysfunction in skeletal muscle: application of intravital video microscopy. *Int. J. Microcirc. Clin. Exp.* 13 (3), 173–186.
- Pries, A. R., Ley, K., and Gaetgens, P. (1986). Generalization of the Fahraeus principle for microvessel networks. *Am. J. physiology* 251 (6 Pt 2), H1324–H1332. doi:10.1152/ajpheart.1986.251.6.H1324
- Renkin, E. M. (1985). B. W. Zweifach Award lecture. Regulation of the microcirculation. *Microvasc. Res.* 30 (3), 251–263. doi:10.1016/0026-2862(85)90057-3
- Riemann, M., Rai, A., Ngo, A. T., Dziegiel, M. H., Holstein-Rathlou, N. H., and Torp-Pedersen, C. (2011). Oxygen-dependent vasomotor responses are conducted upstream in the mouse cremaster microcirculation. *J. Vasc. Res.* 48 (1), 79–89. doi:10.1159/000318777
- Rowell, L. B. (2004). Ideas about control of skeletal and cardiac muscle blood flow (1876–2003): cycles of revision and new vision. *J. Appl. physiology Bethesda, Md. 1985* 97 (1), 384–392. doi:10.1152/japplphysiol.01220.2003
- Russell McEvoy, G. M., Shogan, H., Sové, R. J., and Fraser, G. M. (2021). Development and validation of a novel microfluidic device for the manipulation of skeletal muscle microvascular blood flow *in vivo*. *Microcirc. N. Y. N.Y.* 1994 28 (5), e12698. doi:10.1111/micc.12698
- Russell McEvoy, G. M., Wells, B. N., Kiley, M. E., Kaur, K. K., and Fraser, G. M. (2022). Dynamics of capillary blood flow responses to acute local changes in oxygen and carbon dioxide concentrations. *Front. physiology* 13, 1052449. doi:10.3389/fphys.2022.1052449
- Schubert, R., and Mulvany, M. J. (1999). The myogenic response: established facts and attractive hypotheses. *Clin. Sci. Lond. Engl.* 1979 96 (4), 313–326. doi:10.1042/cs0960313
- Segal, S. S. (1994). Cell-to-cell communication coordinates blood flow control. *Hypertens. Dallas, Tex.* 1979 23 (6 Pt 2), 1113–1120. doi:10.1161/01.hyp.23.6.1113
- Segal, S. S. (2005). Regulation of blood flow in the microcirculation. *Microcirc. New York, N.Y.* 1994 12, 33–45. doi:10.1080/10739680590895028
- Song, H., and Tymk, K. (1993). Evidence for sensing and integration of biological signals by the capillary network. *Am. J. physiology* 265 (4 Pt 2), H1235–H1242. doi:10.1152/ajpheart.1993.265.4.H1235
- Sové, R. J., Fraser, G. M., Goldman, D., and Ellis, C. G. (2016). Finite element model of oxygen transport for the design of geometrically complex microfluidic devices used in biological studies. *PLoS one* 11 (11), e0166289. doi:10.1371/journal.pone.0166289
- Sové, R. J., Milkovich, S., Nikolov, H. N., Holdsworth, D. W., Ellis, C. G., and Fraser, G. M. (2021). Localized oxygen exchange platform for intravital video microscopy investigations of microvascular oxygen regulation. *Front. physiology* 12, 654928. doi:10.3389/fphys.2021.654928
- Sparks, H. V. (1980). Mechanism of vasodilation during and after ischemic exercise. *Fed. Proc.* 39 (5), 1487–1490.
- Sprague, R. S., Ellsworth, M. L., Stephenson, A. H., and Lonigro, A. J. (1996). ATP: the red blood cell link to NO and local control of the pulmonary circulation. *Am. J. physiology* 271 (6 Pt 2), H2717–H2722. doi:10.1152/ajpheart.1996.271.6.H2717
- Sprague, R. S., Hanson, M. S., Achilleus, D., Bowles, E. A., Stephenson, A. H., Sridharan, M., et al. (2009). Rabbit erythrocytes release ATP and dilate skeletal muscle arterioles in the presence of reduced oxygen tension. *Pharmacol. Rep. P. R.* 61 (1), 183–190. doi:10.1016/s1734-1140(09)70020-9
- Stamler, J. S., Jia, L., Eu, J. P., McMahon, T. J., Demchenko, I. T., Bonaventura, J., et al. (1997). Blood flow regulation by S-nitrosohemoglobin in the physiological oxygen gradient. *Sci. (New York, N.Y.)* 276 (5321), 2034–2037. doi:10.1126/science.276.5321.2034
- Stein, J. C., Ellis, C. G., and Ellsworth, M. L. (1993). Relationship between capillary and systemic venous PO₂ during nonhypoxic and hypoxic ventilation. *Am. J. physiology* 265 (2 Pt 2), H537–H542. doi:10.1152/ajpheart.1993.265.2.H537
- Stein, J. C., and Ellsworth, M. L. (1993). Capillary oxygen transport during severe hypoxia: role of hemoglobin oxygen affinity. *J. Appl. physiology (Bethesda, Md. 1985)* 75 (4), 1601–1607. doi:10.1152/jappl.1993.75.4.1601
- Sullivan, S. M., and Johnson, P. C. (1981). Effect of oxygen on blood flow autoregulation in cat sartorius muscle. *Am. J. physiology* 241 (6), H807–H815. doi:10.1152/ajpheart.1981.241.6.H807
- Tateishi, J., and Faber, J. E. (1995a). ATP-sensitive K⁺ channels mediate alpha 2D-adrenergic receptor contraction of arteriolar smooth muscle and reversal of contraction by hypoxia. *Circulation Res.* 76 (1), 53–63. doi:10.1161/01.res.76.1.53
- Tateishi, J., and Faber, J. E. (1995b). Inhibition of arteriole alpha 2- but not alpha 1-adrenoceptor constriction by acidosis and hypoxia *in vitro*. *Am. J. physiology* 268 (5 Pt 2), H2068–H2076. doi:10.1152/ajpheart.1995.268.5.H2068
- Tymk, K., and Budreau, C. H. (1991). A new preparation of rat extensor digitorum longus muscle for intravital investigation of the microcirculation. *Int. J. Microcirc. Clin. Exp.* 10 (4), 335–343.
- Ward, M. E. (1999). Dilation of rat diaphragmatic arterioles by flow and hypoxia: roles of nitric oxide and prostaglandins. *J. Appl. physiology (Bethesda, Md. 1985)* 86 (5), 1644–1650. doi:10.1152/jappl.1999.86.5.1644
- Welsh, D. G., and Segal, S. S. (1998). Endothelial and smooth muscle cell conduction in arterioles controlling blood flow. *Am. J. physiology* 274 (1), H178–H186. doi:10.1152/ajpheart.1998.274.1.H178
- Yuan, S. Y., and Rigor, R. R. (2010). Regulation of endothelial barrier function. *Morgan and Claypool Life Sci.* 3, 1–146. doi:10.4199/c00025ed1v01y201101isp013